UNIVERSITÀ DEGLI STUDI
DI NAPOLI FEDERICO II

HAN-LIANG,LIN

Composite materials for the strengthening of masonry walls

FRP++
Advanced structural analysis and design using composite materials

Master Dissertation
European Master Advanced Structural Analysis and Design using Composite Materials

Work developed under the supervision of
Professor Marta Del Zoppo
Professor Marco Di Ludovico

Funded by the European Union

July 2025

DECLARATION

Name: HAN-LIANG,LIN

Email: pg58211@alunos.uminho.pt **Phone number:** +351913617058

Title of the Thesis: Composite materials for the strengthening of masonry walls

Supervisors:

Professor Marta Del Zoppo

Professor Marco Di Ludovico

Year of Conclusion: 2025

Master Course in Advanced Structural Analysis and Design using Composite Materials

University of Naples Federico II, 21/07/2025

Signature:

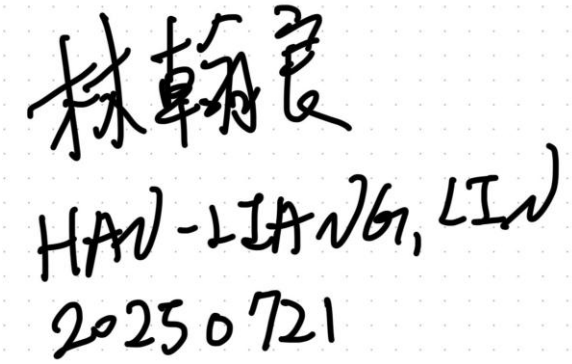

ACKNOWLEDGEMENTS

First, I would like to express my deepest gratitude to the FRP++ research group, especially Professor Sena Cruz and Professor Luís Correia, for giving me the opportunity to join this incredible master's program. I know I may not be the smartest student, but I truly appreciate their trust and support in accepting me as part of the team.

I am especially thankful to my supervisors, Professor Marta and Professor Marco, for their endless patience and kindness. No matter the situation, they were always there to guide me and help me grow, and I will always be grateful for everything they have done.

To my classmates and friends, Hevar, Jacques, Brightworthy, Bollagi, and Raymond—thank you for helping me integrate, encouraging me during difficult times, and making our classes so full of fun and warmth. I will treasure those moments forever.

Finally, I want to thank my mother 陳秋月 and sister 林宜珈 for always supporting my dreams, and my dear friends 蔡深翰, 曾韋霖, 陳星元, 陳家瑜, 林振揚, 連宛勻, and Helene for listening to me, cheering me up, and accepting my emotional ups and downs when I needed it most.

And last but not least, I want to thank myself—I made it.

To my father, 林坤成, I miss you deeply. Rest in peace.

Materiali compositi per il rinforzo delle murature

RIASSUNTO

Questa tesi presenta uno studio analitico e probabilistico completo sul comportamento fuori piano delle murature non armate (URM) rinforzate con sistemi compositi, inclusi i materiali polimerici fibrorinforzati (FRP) e le matrici cementizie fibrorinforzate (FRCM). È stato sviluppato un modello numerico basato sul principio del lavoro virtuale per stimare la capacità flessionale sia delle pareti non rinforzate che di quelle rinforzate, sottoposte ad azioni sismiche e a carichi idrodinamici indotti da tsunami. Il modello identifica automaticamente il meccanismo di collasso dominante—schiacciamento della muratura, rottura delle fibre oppure delaminazione—sulla base delle proprietà del rinforzo e dei parametri geometrici della sezione. L'implementazione è stata realizzata in MATLAB e validata tramite dati sperimentali disponibili, dimostrando un'accuratezza accettabile nella previsione della capacità a flessione e delle modalità di collasso. Il confronto deterministico tra le soluzioni progettuali ha evidenziato che, sebbene i sistemi CFRP offrano una resistenza teorica più elevata, i sistemi FRCM garantiscono prestazioni più stabili e con minore variabilità. Successivamente è stata condotta una simulazione Monte Carlo con 50.000 campioni, al fine di valutare l'affidabilità statistica delle diverse configurazioni di rinforzo. I risultati mostrano che i calcoli deterministici tendono a sovrastimare la capacità delle pareti rinforzate con FRP, con efficienze sperimentali spesso comprese tra il 40% e il 60% del valore progettuale. I risultati probabilistici, compresi i grafici delle funzioni di distribuzione cumulativa (CDF) per le variabili di risposta principali, offrono una solida base per la progettazione basata sull'affidabilità.

In conclusione, lo studio sottolinea l'importanza di integrare nei modelli di carico da tsunami sia i fattori di riduzione sperimentali che le caratteristiche del regime di flusso. La metodologia proposta rappresenta uno strumento utile per la valutazione prestazionale e la pianificazione dell'intervento su murature in contesti soggetti a più tipi di rischio.

PAROLE CHIAVE: Murature non armate (URM); FRP; FRCM; comportamento fuori piano; metodo del lavoro virtuale; carichi da tsunami; simulazione Monte Carlo; progettazione basata sull'affidabilità; capacità flessionale; modalità di collasso.

Composite materials for the strengthening of masonry walls

ABSTRACT

This thesis presents a comprehensive analytical and probabilistic study on the out-of-plane behavior of unreinforced masonry (URM) walls retrofitted with composite strengthening systems, including fiber-reinforced polymer (FRP) and fabric-reinforced cementitious matrix (FRCM). A numerical framework based on the principle of virtual work was developed to estimate the flexural capacity of both unstrengthened and strengthened walls under seismic and tsunami-induced hydrodynamic loading. The model automatically identifies the governing failure mechanism—either masonry crushing and fiber rupture or debonding—based on reinforcement properties and cross-sectional parameters.

The implementation was carried out in MATLAB and validated using available experimental data, demonstrating reasonable accuracy in predicting moment capacity and failure trends. A deterministic design comparison showed that while CFRP systems exhibit higher theoretical strength, FRCM systems offer more stable performance with reduced variability. A Monte Carlo simulation with 50,000 samples was then conducted to evaluate the statistical reliability of different retrofitting configurations. The results indicate that deterministic calculations tend to overestimate the capacity of FRP-retrofitted walls, with experimental efficiency often ranging between 40% and 60% of the design value. The probabilistic outputs, including the Fragility Function for key response variables, provide a robust basis for reliability-based design. Ultimately, the study emphasizes the significance of incorporating experimental reduction factors and flow regime considerations into tsunami scenarios. The proposed methodology offers a valuable tool for performance-based assessment and retrofit planning of masonry walls in multi-hazard environments.

KEYWORDS: URM walls; FRP; FRCM; Out-of-plane behavior; Virtual work method; Tsunami loading; Monte Carlo simulation; Reliability-based design; Flexural capacity; Failure mechanism.

TABLE OF CONTENTS

LIST OF FIGURES

LIST OF TABLES

LIST OF ABBREVIATIONS AND SYMBOLS

Abbreviations

RC	Reinforced concrete
URM	Unreinforced masonry
FRP	Fibre Reinforced Polymer
CFRP	Carbon Fibre Reinforced Polymer
FRCM	Fiber Reinforced Cementitious Matrix
TRM	Textile-Reinforced Mortar

Symbols

Uppercase Roman Letters

A_f	Area of FRP/FRCM reinforcement
E_m	Masonry elastic modulus
E_f	FRP/FRCM elastic modulus
F'_f	Force resultants for FRCM in tension
F'_m	Force resultants for masonry in compression
H_w	Flood/Tsunami high
k_{Gk}	Characteristic value of the calibrated dimensionless coefficient
L_i	Internal virtual work
L_E	External virtual work
L_P	External virtual work of axial load
M_R^{UR}	Flexural strength of the unreinforced masonry wall
M_R	Flexural strength of the FRCM reinforced wall
M_{Rd}	Design out-of-plane flexural strength of the FRCM strengthened masonry
N	Resultant compressive stress in the vertical arch per unit length
P	Design axial force acting on the section
P_t	Hydrodynamic pressure on the top
P_b	Hydrodynamic pressure on the bottom.
P_m	Hydrodynamic pressure on the middle.
$R1$	Resulting forces for the external load distribution
$R2$	Resulting forces for the external load distribution

W	Walls length
X_d	Design value of generic property
R_d	Characteristic value of generic property

Lower Roman Letters

c'	Neutral axis depth theory
c	Neutral axis depth real situation
c_c	Compressive zone
d	OOP displacement of the infill center
f_f	Strength of FRP/FRCM reinforcement
f_{fd}	Design strength of FRP/FRCM reinforcement
f_{fdd}	Mean debonding strength of FRP reinforcement
f_{mc}	Masonry compressive strength
g	Gravity
n_l	Number of layers
n_s	Number of strip
h	Walls high
$h1$	Distances of resulting forces from the edges of the wall.
$h2$	Distances of resulting forces from the edges of the wall
$k1$	Stress block parameter
$k2$	Stress block parameter
k_b	Geometric coefficient
s_u	Interface slip corresponding to complete debonding from the substrate.
t	Walls thickness
t_f	Thickness of the FRP/FRCM reinforcement
w_f	Width of a single strip in the FRP/FRCM reinforcement system

Greek Letters (Uppercase)

Γ_{Fk}	characteristic value of the maximum bond stress at the FRP-masonry interface

Greek Letters (Lowercase)

β	Stress block parameter
γ	Stress block parameter

γ_f	Partial factor
γ_{f2}	Partial factor
γ_h	Ratio for horizontal load application high
ε_{fdd}	Maximum design strain in FRP/FRCM due to end debonding
ε_{fd}	Maximum design strain in FRP/FRCM reinforcement
εf_e	Effective tensile strain in FRCM
ε_{fk}	Characteristic strain at tensile failure of FRP reinforcement
ε_{mu}	Ultimate compressive strain of confined masonry
η	Conversion factor
η_a	Environmental conversion factor
η_l	Longterm conversion factor
ρ	Seawater density
ρ_f	FRP reinforcement ratio
ρ_{fb}	Balanced reinforcement ratio
φ	Rotation of infill parts

1. INTRODUCTION

1.1. Introduction

The history of composite materials dates back to ancient times. For instance, the ancient Egyptians used sun-dried bricks made from a mixture of mud, straw, and papyrus. In contrast, the ancient Assyrians engineered composite bows using layers of wood, sinew, and horn—early examples of structural composites
[1][2] , as depicted in Figure 1.1-1 and Figure 1.1-2. These practices represent the earliest conceptual uses of engineered composite systems.

Figure 1.1-1 Bricks made of mixed straws with mad.

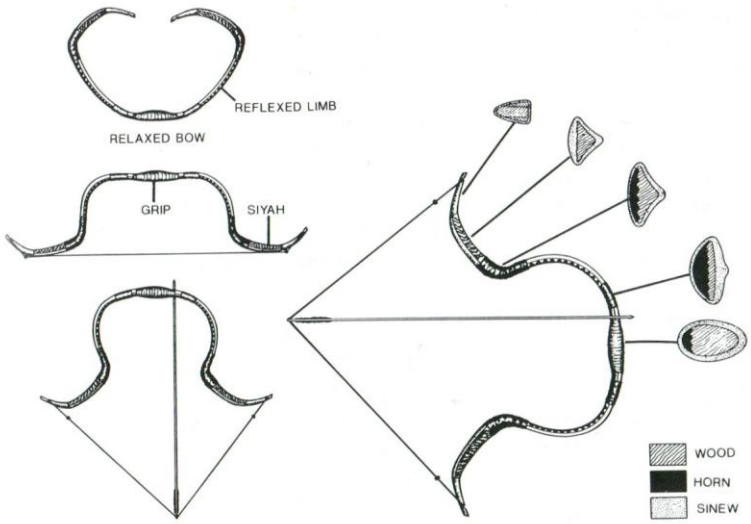

Figure 1.1-2 Composite bows.

Since the mid-20th century, the development of synthetic composite materials has expanded rapidly, particularly following the invention of fiberglass in the 1930s and the subsequent use of carbon fiber and aramid fiber composites in the aerospace and automotive industries[3][4]. Today, composite materials are utilized to construct stronger and lighter structures across various fields, including civil engineering, transportation, and space exploration. As research continues to advance, the applications of composite materials continue to expand[5][6], as depicted in Figure 1.1-3.

Given the growing application of composite materials in the field of civil engineering, they have become widely adopted for the retrofitting and strengthening of buildings, bridges, and historical monuments.

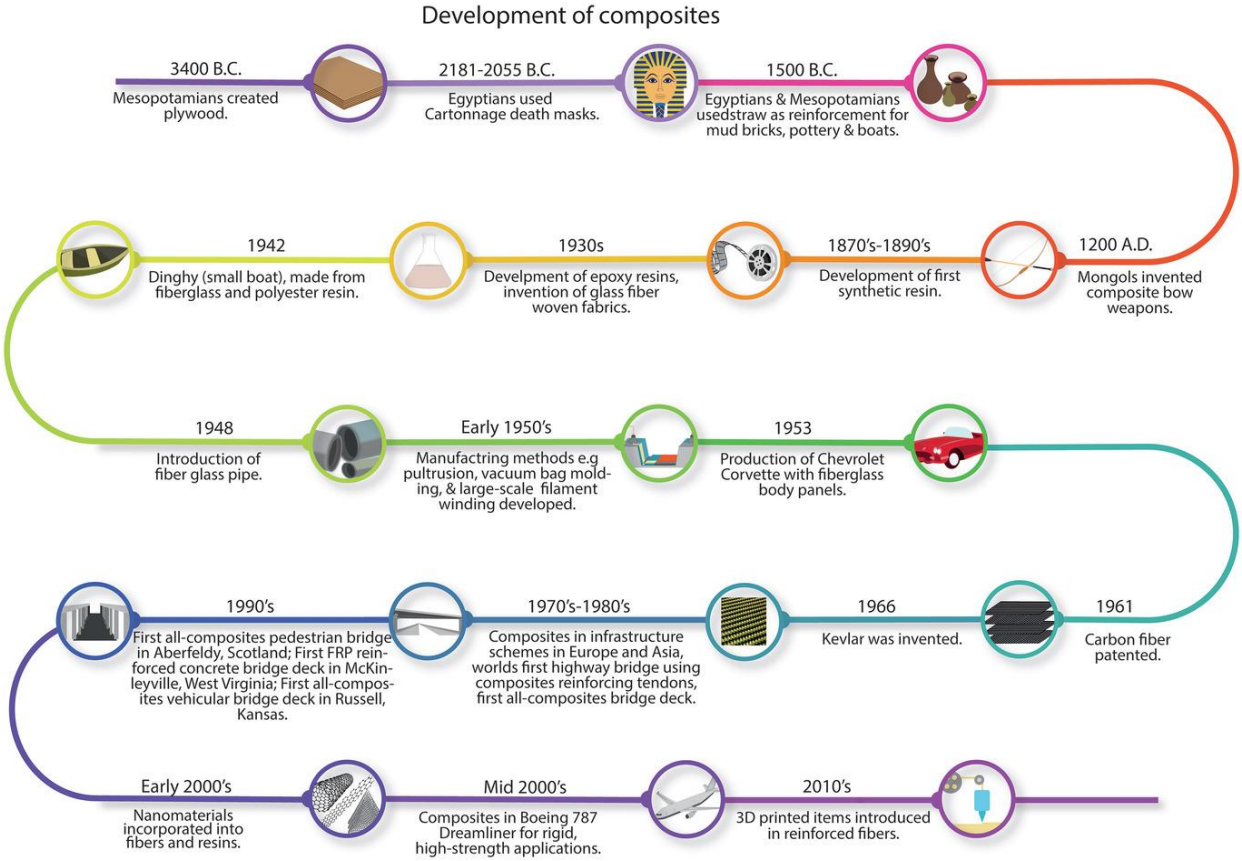

Figure 1.1-3 Chronological development of composites manufacturing for several industries [7].

The author of this thesis is a Taiwanese student currently studying in Italy. Notably, both Taiwan and Italy are seismically active regions that frequently experience earthquakes and related natural disasters. In addition to seismic risks, both countries are surrounded by oceanic environments, making them equally vulnerable to hazards such as floods and tsunamis. These

shared geographic and environmental conditions underscore the pressing need for practical, reliable, and sustainable structural reinforcement techniques.

In response to these challenges, this thesis focuses on the out-of-plane behavior of masonry walls, particularly their damage mechanisms under seismic and tsunami-induced loads. A simplified yet practical strengthening method using composite materials is proposed and evaluated through analytical modeling, with comparisons to recent experimental and literature-based references.

1.2. Motivation

Compared to reinforced concrete (RC) structures, masonry walls typically lack internal steel reinforcement , as depicted in Figure 1.2-1 and Figure 1.2-2. As a result, they have significantly lower ductility and are more susceptible to brittle failure. When damage occurs, their behavior can be sudden and unpredictable, which poses a serious challenge to structural safety and reliability during seismic events or other extreme loading situations.

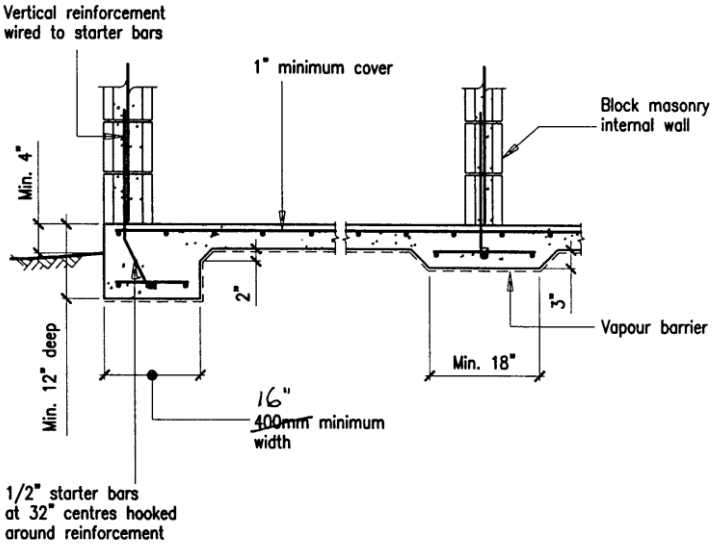

Figure 1.2-1 RC wall typical cross section showing concrete with internal reinforcement.[8]

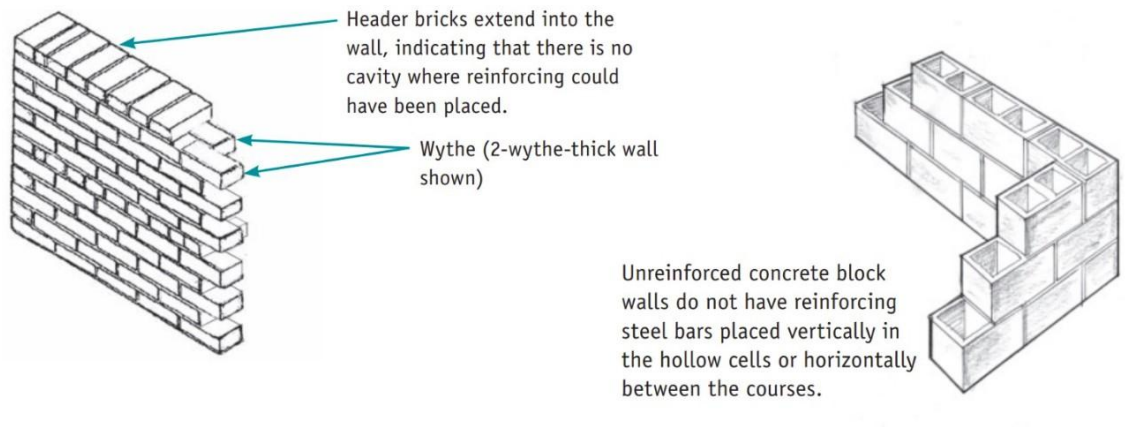

Figure 1.2-2 URM wall cross section without reinforcement.[9]

Many existing masonry walls, especially those found in historical or rural areas, were not built according to modern design codes, such as the Eurocode. In some cases, no formal standards were followed during the construction process. This situation increases their vulnerability and raises the likelihood of unexpected failure.

The 1999 Chi-Chi Earthquake in Taiwan and the 2009 L'Aquila Earthquake in Italy underscored the critical need for practical and effective retrofitting solutions, as demonstrated by the extensive damage to unreinforced masonry buildings. These earthquakes not only resulted in structural collapses but also caused significant cultural and economic losses. In many instances, damaged buildings had heritage value, making traditional intrusive strengthening methods inappropriate,as depicted in Figure 1.2-3 and Figure 1.2-4.

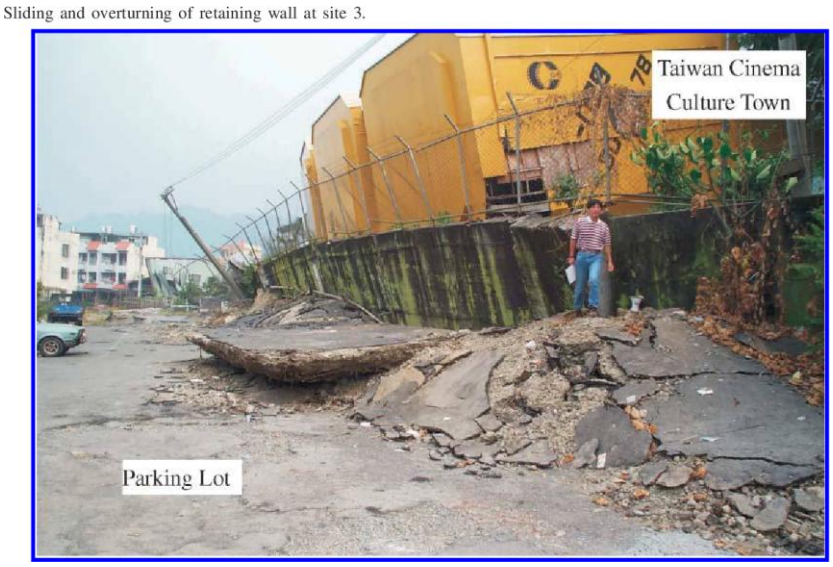

Figure 1.2-3 Sliding and overturning of a retaining wall in Taiwan during the 1999 Chi-Chi Earthquake.[10]

Figure 1.2-4 Collapse of unreinforced masonry buildings in the historical center after the 2009 L'Aquila Earthquake, Italy.[11]

Composite materials provide an innovative solution due to their high strength-to-weight ratio, ease of application, and compatibility with existing masonry. When properly designed, such systems can enhance out-of-plane flexural performance, delay crack initiation, and improve post-peak ductility while preserving the building's original character.

Retrofitting with composite materials not only improves resilience but also significantly reduces the risk of sudden collapse and related accidents, thereby contributing to overall safety and post-disaster recovery.

1.3. Objectives of the research

The primary objective of this research is to assess the out-of-plane performance of masonry walls subjected to seismic and tsunami-induced loads and to evaluate the effectiveness of utilizing composite materials, such as FRP (Fiber Reinforced Polymer) and FRCM (Fiber Reinforced Cementitious Matrix), in enhancing their flexural capacity and overall structural behavior.

This research addresses the gap between analytical theory and practical application by integrating numerical models with design standards, thereby empowering engineers with reliable tools. Our goal is to assist them in assessing existing vulnerabilities and exploring the potential benefits of retrofitting.ultimately contributing to safer and more resilient structures for everyone.

Accordingly, the specific objectives of this study are as follows:

A. To calculate the external and ultimate out-of-plane forces acting on unstrengthened masonry walls and to compare the results with available experimental data.
B. To design an appropriate retrofitting process based on the guidelines provided in CNR-DT standards.
C. To investigate the performance of different composite strengthening materials, including FRP, FRCM, and others.
D. To validate theoretical predictions through comparison with experimental results.

1.4. Thesis outline

This thesis is structured into seven chapters, each addressing a key component of the research framework:

1. Chapter 1 introduces the background, research motivation, and objectives, along with the scope and methodology adopted.
2. Chapter 2 presents a comprehensive review of existing literature on the out-of-plane behavior of URM walls, strengthening techniques using FRP/FRCM systems, and numerical modeling approaches, including the virtual work method.
3. Chapter 3 details the development of the analytical model based on the principle of virtual work, incorporating both unstrengthened and retrofitted wall scenarios under seismic and tsunami loading.
4. Chapter 4 describes the implementation of the proposed model in MATLAB, including parameter calibration, failure mode identification, and output validation.
5. Chapter 5 compares deterministic simulation results with available experimental data to assess the accuracy and predictive capability of the model for different strengthening configurations.
6. Chapter 6 conducts a probabilistic Monte Carlo analysis to evaluate the statistical distribution of key response parameters and the reliability of strengthened walls under variable conditions.
7. Chapter 7 summarizes the key findings, discusses design implications, and proposes future research directions to enhance the applicability of the proposed framework in multi-hazard contexts.

2. LITERATURE REVIEW

2.1.Strengthening Strategies and Materials for Existing Masonry Walls

The structural vulnerability of unreinforced masonry (URM) walls under seismic, tsunami, or out-of-plane loading has been extensively documented. Historical and non-engineered masonry constructions often lack sufficient ductility and structural continuity, making them particularly susceptible to brittle and sometimes sudden failure when subjected to lateral or hydrodynamic forces. Tsunami-induced loading, including both hydrostatic pressure and hydrodynamic surge, can generate substantial out-of-plane forces on masonry infill or boundary walls. These factors highlight the urgent need for effective and minimally invasive retrofit techniques, especially in seismically active or coastal hazard-prone areas.

To address these structural deficiencies, several strengthening strategies have been proposed. Among them, externally bonded Fiber-Reinforced Polymer (FRP), Fabric-Reinforced Cementitious Matrix (FRCM), and Textile-Reinforced Mortar (ratio) systems have gained prominence due to their effectiveness in enhancing the out-of-plane flexural capacity, ductility, and overall stability of URM walls without significantly altering their architectural appearance or adding excessive dead load , as supported by previous studies [12][13] and depicted in Figure 2.1-1 and Figure 2.1-2 .

(a) FRP strengthening (b) FRCM strengthening

Figure 2.1-1 Different ways to retrofit masonry walls

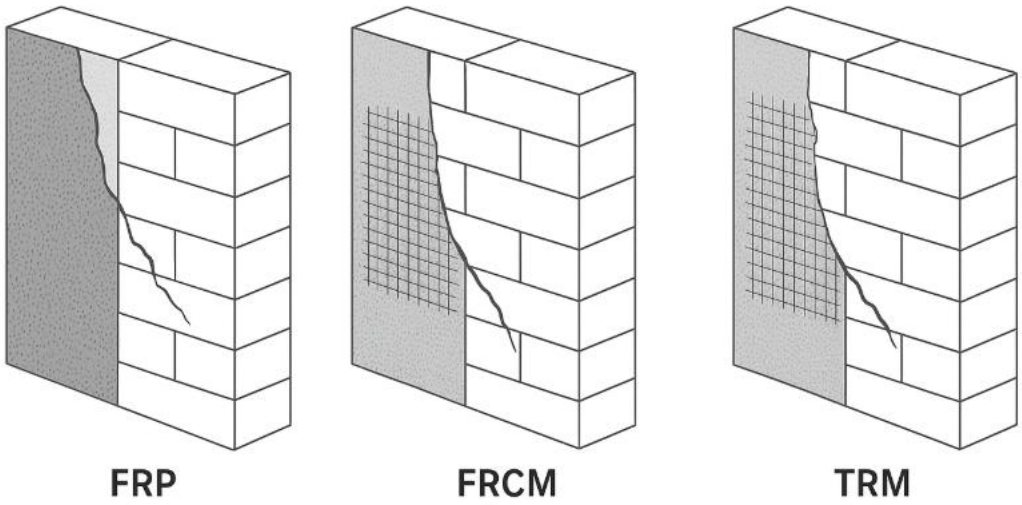

Figure 2.1-2 Comparison of composite retrofitting techniques for URM walls: FRP, FRCM, and TRM systems.

Experimental studies by Borri et al. [14] and Ricci et al. [15] demonstrated that such composite systems can effectively delay crack propagation and improve both ultimate load capacity and post-elastic deformation behavior. Recent studies, particularly those by Triantafillou and Koutas [16], demonstrate that properly preparing the surface and detailing the anchorage is crucial for achieving good composite action. However, concerns remain about long-term durability, particularly when these methods are applied to historic structures constructed from weak or moisture-sensitive materials.

FRP systems consist of high-strength fibers (such as carbon, glass, or basalt) embedded in a polymeric resin matrix. These systems are widely recognized for their high strength-to-weight ratio and ease of installation. They are particularly effective in improving the shear and flexural capacities of masonry walls. However, the polymeric matrix of FRP is sensitive to fire, high temperatures, and ultraviolet radiation. Additionally, failure modes such as fiber rupture and debonding are often brittle, which could jeopardize the long-term reliability of the retrofitted system [17][18][19] , and depicted in Figure 2.1-3.

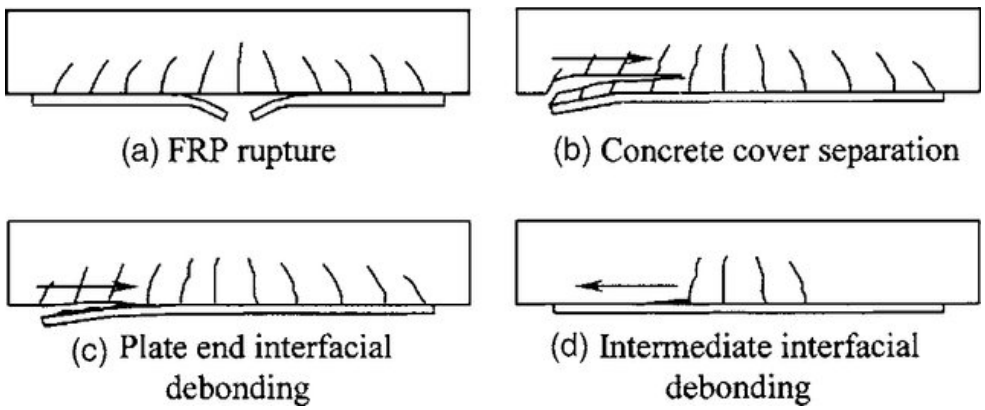

Figure 2.1-3 FRP-related failure modes of RC beams strengthened by FRP plate.[20]

FRCM systems incorporate fiber meshes within inorganic cementitious matrices, which enhances breathability, fire resistance, UV stability, and material compatibility with existing or historical masonry. These attributes make FRCM a more favorable option for heritage retrofitting. Despite its improved ductility compared to FRP, FRCM systems can still experience premature failure due to fiber slippage and mortar cracking. The overall performance of FRCM is, therefore, sensitive to installation quality and environmental conditions [21][22][23][24] , and depicted in Figure 2.1-4.

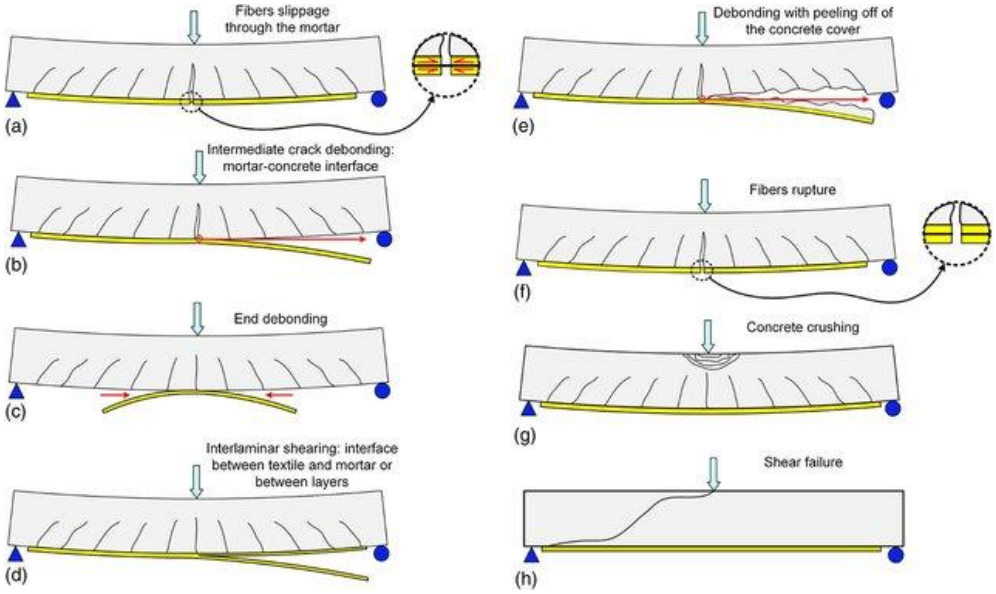

Figure 2.1-4 Failure modes of RC elements strengthened in flexure with FRCM.[25]

TRM is a specialized variant of FRCM, using textile fibers (e.g., glass, carbon, or basalt) embedded in specially formulated mortar. TRM systems offer excellent bond performance, greater flexibility, and improved adaptability, which are particularly beneficial for retrofitting complex geometries or surfaces in heritage structures. Additionally, TRM exhibits high thermal stability and environmentally friendly characteristics during installation. However, the structural effectiveness of TRM remains limited by the mechanical properties of the textile mesh and mortar matrix, and further experimental and numerical studies are needed to validate its long-term performance [26][27][28][29].

In summary, the selection of a suitable retrofitting material system should be based on structural requirements, durability expectations, and compatibility with existing materials. FRP systems are typically chosen for fast, high-strength upgrades. In contrast, FRCM and TRM are more appropriate for historic conservation projects or when long-term exposure to temperature, moisture, or fire is a concern [30][31].

A comparative Table 2-1 summarizes the key features, benefits, limitations, and application contexts of FRP, FRCM, and TRM systems for easier selection. This table serves as a practical

reference for engineers and researchers to choose the most appropriate strengthening strategy based on specific project demands [32][33][34][35][36].

Table 2-1 Comparative Summary of Composite Strengthening Systems for Masonry Walls

Feature	**FRP(Fiber-Reinforced Polymer)**	**FRCM(Fabric-Reinforced Cementitious Matrix)**	**TRM(Textile-Reinforced Mortar)**
Fiber Types	Carbon, Glass, Basalt [35]	Carbon, Glass, Basalt [36]	Glass, Carbon, Basalt textiles [32]
Matrix Material	Organic (typically epoxy resin) [35]	Inorganic cementitious mortar [36]	Mineral-based mortar [32][33]
Main Advantages	High tensile strength, light weight, easy installation [35]	Vapor-permeable, fire- and UV-resistant, good compatibility with old masonry [33] [36]	Flexible, reversible, and suitable for heritage conservation [32][33]
Historical Suitability	Limited–not breathable, may trap moisture in old masonry [35]	High – compatible with historical materials [33][36]	Very high – suitable for curved or delicate structures [32][33]
Durability	Sensitive to fire, UV, and high temperature [35]	Good resistance to environmental exposure [33][34]	Excellent resistance to moisture, heat, and aging [32][33]
Failure Modes	Fiber rupture, debonding at interface [34] [35]	Fiber slippage, matrix cracking [34][36]	Mortar–textile delamination or deterioration over time [32][33]
Typical Application	Rapid strengthening in modern buildings or bridges [35]	Structural retrofitting in historical or moisture-sensitive masonry [33][36]	Retrofitting of curved surfaces or heritage assets requiring reversibility [32][33]
Design Standards	CNR-DT 200 R2/2025, ACI 440 [35]	CNR-DT 215/2018 [36]	CNR-DT 215/2018, national heritage restoration guidelines [32][36]

2.2. Virtual Work-Based Analysis of URM Walls

The evaluation of the out-of-plane (OOP) capacity of unreinforced masonry (URM) walls is a crucial aspect of seismic and tsunami-resistant design, particularly for slender or infill wall systems. Over the past few decades, various analytical models have been proposed to estimate the out-of-plane flexural resistance of masonry walls subjected to lateral loading. Among these, the yield line theory and the arch mechanism approach are the most widely adopted.

One of the most influential and widely cited analytical models is that developed by Dawe and Seah (1989) [37], who applied the principle of virtual work to derive closed-form expressions for the out-of-plane capacity of masonry panels. Their model treats the masonry wall as a homogenous, linearly elastic-perfectly plastic plate and assumes the development of plastic hinges along predicted failure lines. The primary advantage of this approach lies in its simplicity and ability to accurately capture the mechanical behavior of URM walls subjected to lateral loads, utilizing only basic geometric parameters and material properties.

Dawe and Seah's model primarily considers a one-way vertical arching mechanism, wherein a single horizontal yield line forms near the mid-height of the wall. The internal and external virtual work are balanced to determine the collapse load. Their methodology is particularly suited for infill walls restrained at the top and bottom, and its accuracy has been reasonably validated through experimental results, as depicted in Figure 2.2-1.

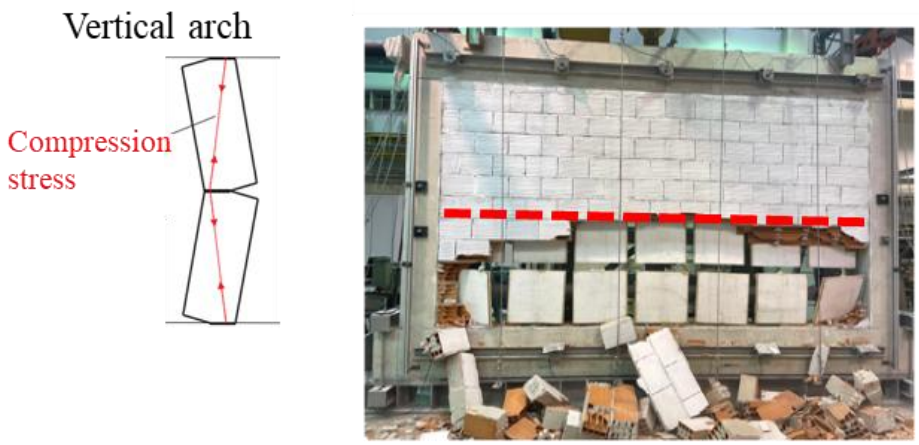

Figure 2.2-1: One-way arching failure mechanism.

Although the original model assumes ideal support conditions and uniform loading, it serves as a foundational reference for further analytical developments. In most real-world applications, engineers must adapt the model to account for partial fixity at the boundaries, non-uniform loading, and the presence of axial forces. These adaptations enable the method to better approximate the behavior of actual wall configurations and improve its predictive reliability.

In recent years, the virtual work framework initially developed by Dawe and Seah has been extended to analyze the out-of-plane response of walls subjected to non-seismic lateral loads, such as blast waves and tsunami surges, demonstrating the versatility and theoretical robustness of this method [38]. These extensions account for different force distributions (e.g., hydrostatic vs. hydrodynamic profiles) and the time-dependent nature of transient loading, further validating the approach for multi-hazard analysis.

For practical engineering design, the virtual work method provides a valuable analytical tool that can deliver rapid estimates of collapse loads, especially in preliminary assessment or retrofit feasibility studies. Despite its idealized assumptions, it serves as a benchmark model against which more sophisticated finite element or experimental data can be compared.

2.3. Out-of-Plane Loading Mechanisms in Seismic and Tsunami Events

Unreinforced masonry (URM) walls are highly susceptible to out-of-plane (OOP) failure due to their low tensile strength and lack of reinforcement. During seismic or tsunami events, the mechanisms through which out-of-plane (OOP) loads develop are distinct and require specific attention when assessing structural vulnerability or planning retrofitting strategies.

In seismic events, out-of-plane loads primarily arise from inertial forces induced by ground motion. As floor or roof diaphragms oscillate, they exert dynamic pressures on walls perpendicular to the direction of motion. These inertial loads can cause rocking, cracking, and even full collapse of slender or poorly anchored walls. Experimental work by Griffith and Vaculik [39] and analytical studies by Doherty et al. [40] confirmed that moderate seismic motions are sufficient to trigger these failure modes, especially in the absence of proper diaphragm-wall connections.

These seismic-induced OOP demands often interact with in-plane actions, reducing stability and complicating the structural response. Out-of-plane collapse has been widely reported in past earthquakes, particularly in older masonry structures lacking effective anchorage as depicted in Figure 2.3-1.

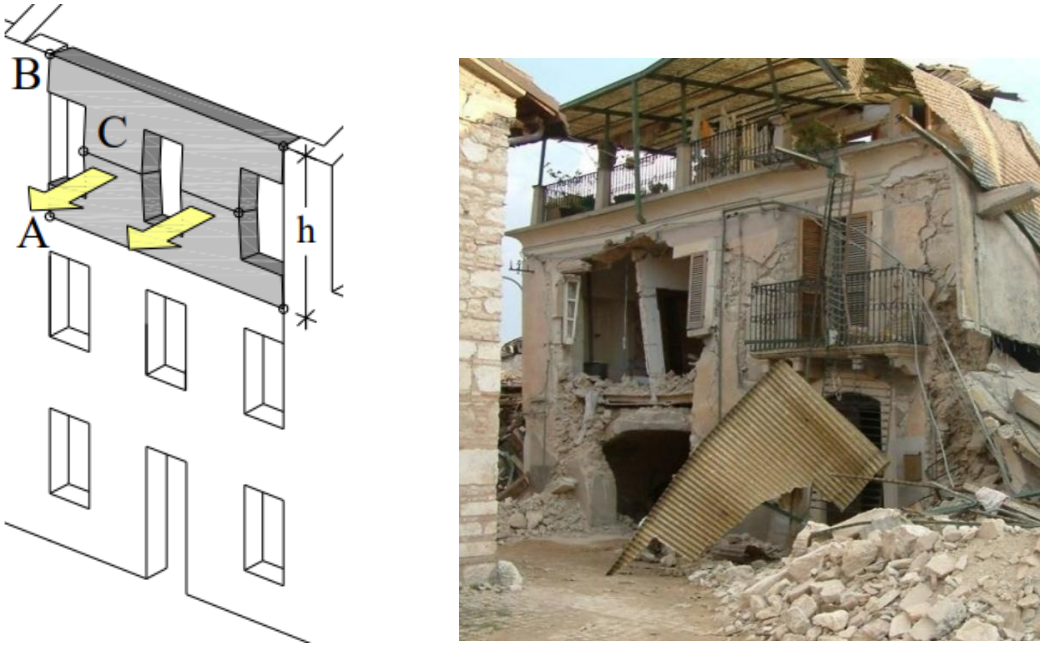

Figure 2.3-1 Failure mode in masonry building during earthquake.

In contrast, tsunami loading involves quasi-static forces with different physical origins. When a tsunami wave hits a structure, it imposes both hydrostatic pressure (due to water depth) and hydrodynamic pressure (from wave velocity) as depicted in Figure 2.3-2.

According to Kafle et al. [41], these forces include:

A. Hydrostatic pressure from the standing water level.
B. Hydrodynamic drag due to wave movement.
C. Bore impact and impulsive surge loading.
D. Debris impact forces.
E. Buoyancy effects, which reduce the effective self-weight of walls.

Compared to seismic forces, tsunami-induced loads are more sustained and may reach higher magnitudes, especially in coastal low-rise structures with large exposed wall areas. Chock et al. [42] emphasize the importance of accounting for both steady and transient components of tsunami flow in structural design.

Natural disasters like earthquakes can lead to further damage, such as tsunamis. For example, cracks from an earthquake can weaken a wall, making it more likely to fail when a tsunami hits. This shows why we need retrofitting solutions that can handle multiple hazards.

Figure 2.3-2 Failure mode in masonry building during tsunami.

2.4.Code-Based Approaches for Retrofitting and Out-of-Plane Design

Retrofitting of masonry structures, particularly for out-of-plane (OOP) behavior, has been addressed in several national and international codes. These include Italian guidelines (CNR-DT 200/201/215), Eurocode 8 Part 3, and U.S. FEMA documents. Each of these provides a practical framework for evaluating structural safety and designing effective strengthening solutions.

A simplified comparison of these three major code-based approaches is provided in Table 2-2 to highlight their key features and differences in OOP strengthening design.

2.4.1. Italian Guidelines: CNR-DT 200 and 215

In the Italian technical framework, composite strengthening systems are addressed in distinct documents depending on the type of matrix. CNR-DT 200 R2/2025 covers externally bonded Fiber-Reinforced Polymer (FRP) systems, outlining their mechanical characterization, durability considerations, design stress limits, and failure modes, including debonding and fiber rupture. On the other hand, CNR-DT 215/2018 is dedicated explicitly to Fiber-Reinforced Cementitious Matrix (FRCM) systems. It defines the design procedures for both in-plane and out-of-plane strengthening, including flexural strength verification, safety factors, anchorage

detailing, minimum reinforcement ratios, and expected failure mechanisms such as fiber slippage or masonry crushing.

In this thesis, all FRP-related retrofitting calculations and verifications are carried out in accordance with the provisions of CNR-DT 200. At the same time, the FRCM-based designs strictly follow the guidelines presented in CNR-DT 215/2018.

2.4.2. Eurocode 8 – Part 3

Eurocode 8 Part 3 provides general provisions for the seismic assessment and retrofitting of existing structures across Europe. For URM walls, it permits the use of simplified force-based methods or equivalent frame modeling to evaluate out-of-plane resistance. Although Eurocode does not explicitly define FRP, FRCM, or TRM systems, it allows engineers to incorporate such technologies under a capacity-based design framework, usually supplemented by national annexes or additional standards.

2.4.3. FEMA Guidelines (USA)

In the United States, FEMA P-2006 and FEMA P-807 focus on the seismic rehabilitation of existing masonry buildings. These documents identify configurations that may lead to collapse and recommend performance-based retrofitting strategies to mitigate these risks. They also emphasize the importance of diaphragm-to-wall anchorage, the interaction between in-plane and out-of-plane responses, and expected failure mechanisms in URM walls.

2.4.4. Common Design Considerations

Despite differences in regional codes, several fundamental design principles are emphasized consistently across all major standards. These include the requirement to ensure adequate anchorage of masonry walls to diaphragms and adjacent elements, as well as the need to assess both local (panel-level) and global (building-level) stability under seismic or tsunami demands. Flexural capacity must be verified using appropriate safety factors that account for material variability and uncertainty. For heritage structures, retrofitting must also address environmental durability, compatibility with historical materials, and the potential for reversibility to maintain both structural integrity and cultural significance over time.

Table 2-2 Comparison of code-based approaches for retrofitting and out-of-plane design of masonry walls.

Aspect	CNR-DT 200/215 (Italy)	Eurocode 8 Part 3 (Europe)	FEMA P-2006/P-807 (USA)
System Types	FRP (CNR-DT 200) FRCM (CNR-DT 215)	General approach; FRP/FRCM not explicitly defined	URM walls; compatible with modern/traditional methods
Design Focus	Strength check, failure modes, anchorage	Seismic evaluation, simplified/advanced analysis	Collapse prevention, IP/OOP interaction
Approach	Safety factor–based design	Capacity-based methods	Performance-based design
OOP Design	Explicit flexural design and failure mode evaluation	Panel or equivalent frame methods	Emphasis on wall–diaphragm anchorage compatibility
Historical Structures	FRCM allowed; reversible & compatible materials	Minimal intervention recommended	Retrofit should be reversible and low-invasive
Durability	Environmental effects addressed in FRP/FRCM design	Considered generally; relies on national annex	Not specified; addressed in detailing

2.5.Summary

This chapter reviewed the current knowledge and engineering practices related to the out-of-plane behavior and retrofitting of unreinforced masonry (URM) walls. The discussion covered structural vulnerabilities under seismic and tsunami actions, retrofitting strategies using FRP, FRCM, and TRM systems, and the application of analytical tools such as the virtual work method. In addition, relevant international design codes (CNR, Eurocode, FEMA) were presented to contextualize retrofitting procedures under different regulatory frameworks.

The literature confirms the high susceptibility of URM walls to out-of-plane collapse, particularly in structures lacking proper anchorage or built without modern standards. Composite strengthening systems have significant potential to enhance both flexural strength and durability while maintaining architectural integrity. However, the effectiveness of these

systems largely depends on proper detailing, material compatibility, and environmental conditions.

The upcoming chapters will apply these insights for analytical modeling and design procedures, intending to validate retrofitting strategies by comparing them with experimental data and calculations based on codes.

THIS PAGE WAS INTENTIONALLY LEFT BLANK

3. METHODOLOGY / ANALYSIS FRAMEWORK

3.1. Analytical Models for Unstrengthened URM Walls

This section presents the analytical procedure based on the principle of virtual work, originally proposed by Dawe and Seah (1989) [37], to evaluate the out-of-plane flexural capacity of unreinforced masonry (URM) walls. The model assumes a one-way arching mechanism and integrates the effects of axial load and lateral displacement.

3.1.1. Virtual Work Principle under Seismic Loading

In seismic scenarios, unstrengthened URM walls are subjected to lateral inertial forces. The collapse mechanism can be analyzed by balancing the internal and external virtual work, as depicted in Figure 3.1-1

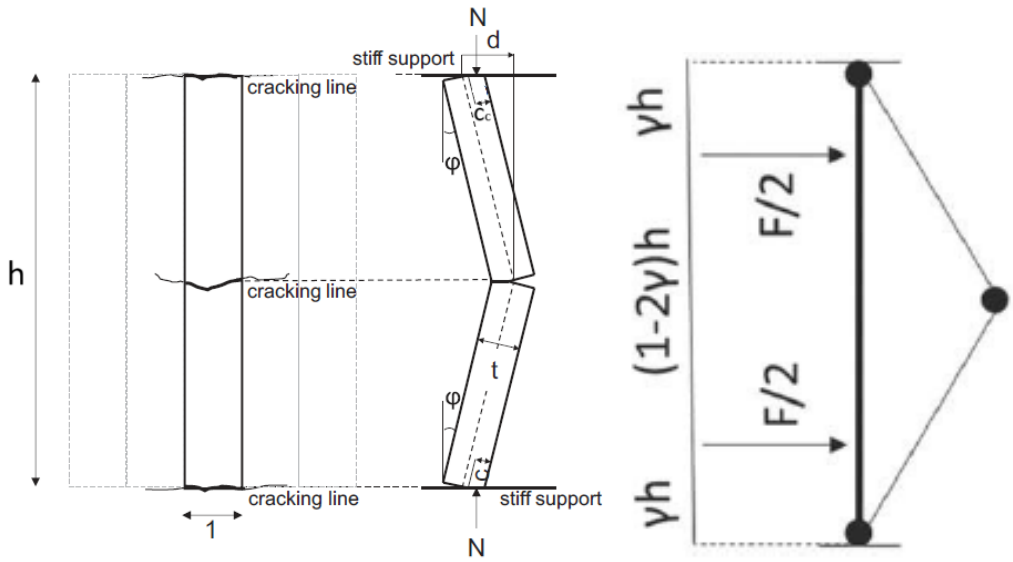

Figure 3.1-1: One-way arching action.

The rotation angle is defined as:

$$\varphi = \frac{2 \times d}{h} \tag{3.1.1-1}$$

The compression zone depth is evaluated using:

$$c_c = \frac{2 \times t \times tan\varphi - h \times (1 - cos\varphi)}{4 \times tan\varphi + (\frac{k_1 \times k_2 \times f_{mc} \times h}{t \times E_m}) \times cos\varphi} \tag{3.1.1-2}$$

The internal work performed by the wall section is:

$$L_i = 2 \times N \times (t - c_c - d) \times W \times \varphi = 4 \times M \times \varphi \quad (3.1.1\text{-}3)$$

$$N = k_1 \times k_2 \times f_{mc} \times c_c \quad (3.1.1\text{-}4)$$

N is the resultant compressive stress in the vertical arch per unit length,M is maximum moment per unit width along the fracture

lines, k_1 and k_2 are stress block parameters both equal to 0.85.

The external virtual work associated with the axial load is:

$$L_P = P \times (t - c_c - d) \times W \times \varphi \quad (3.1.1\text{-}5)$$

The external virtual work due to lateral load is:

$$L_E = F \times \gamma h \times \varphi \quad (3.1.1\text{-}6)$$

The collapse occurs when total external work equals internal work:

$$L_{i,max} = L_E + L_P \quad (3.1.1\text{-}7)$$

The corresponding maximum lateral force can then be determined as:

$$F_{max} = \frac{4}{\gamma h} \times M \times W \quad (3.1.1\text{-}8)$$

3.1.2. Virtual Work Principle under Tsunami and flood Loading

Tsunami loading involves both hydrostatic and hydrodynamic forces. Depending on water depth H_w Different force distributions and moments are calculated, as depicted in Figure 3.1-2.

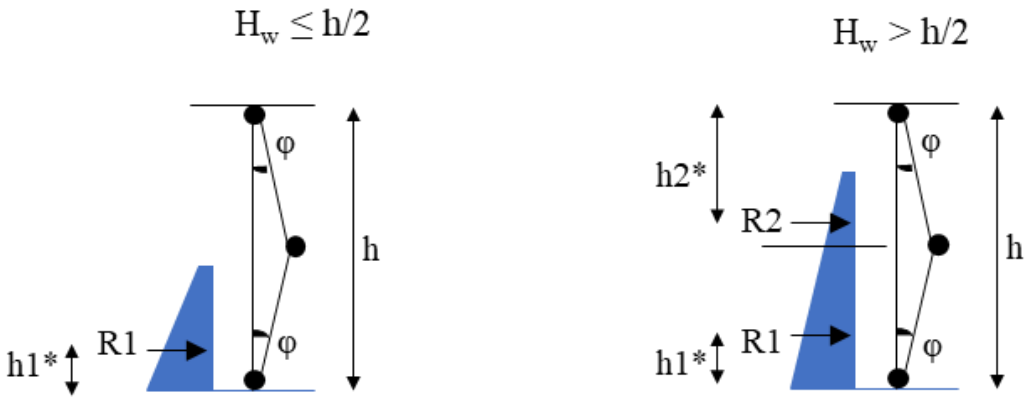

Figure 3.1-2 Virtual works for the vertical arch mechanism.

For $H_w \leq \frac{h}{2}$, the resultant force and distances of resulting forces from the edges of the wall are:

$$R_1 = \frac{(P_t + P_b) \times H_w}{2}, h_1 = \frac{(2 \times P_t + P_b) \times H_w}{3 \times (P_t + P_b)} \quad (3.1.2\text{-}1)$$

$$R_2 = 0, h_2 = 0 \quad (3.1.2\text{-}2)$$

For $H_w > \frac{h}{2}$, the resultant force and distances of resulting forces from the edges of the wall are:

$$R_1 = \frac{(P_m+P_b)\times\frac{H}{2}}{2}, h_1 = \frac{(2\times P_m+P_b)\times\frac{H}{2}}{3\times(P_m+P_b)} \quad (3.1.2\text{-}3)$$

$$R_2 = \frac{(P_t+P_m)\times(H_w-\frac{H}{2})}{2}, h_2 = \frac{H}{2} - \frac{(H_w-\frac{H}{2})\times(2\times P_t+P_m)}{3\times(P_t+P_m)} \quad (3.1.2\text{-}4)$$

For the pressure of the bottom and middle of the wall are:

$$P_m = P_t + \rho \times g \times (H_w - \frac{H}{2}) \times W \quad (3.1.2\text{-}5)$$

$$P_b = P_t + \rho \times g \times H_w \times W \quad (3.1.2\text{-}6)$$

The equations governing the hydrostatic and hydrodynamic loads applied to the wall are expressed as follows:

$$\mathrm{F_s} = 0.5 \times \rho \times g \times W \times \mathrm{H_w}^2 \quad (3.1.2\text{-}7)$$

$$\mathrm{F_d} = 0.5 \times \mathrm{C_D} \times \rho \times \mathrm{W} \times \mathrm{v}^2 \times \mathrm{H_w}, if\ Fr < 1 \quad (3.1.2\text{-}8)$$

$$\mathrm{F_d} = \lambda \times \rho \times \mathrm{W} \times \sqrt[3]{\mathrm{g}} \times \sqrt[3]{(\mathrm{v} \times \mathrm{H_w})^4}, if\ Fr \geq 1 \quad (3.1.2\text{-}9)$$

$$\mathrm{v} = \frac{\mathrm{Fr}}{\sqrt{\mathrm{g}\times\mathrm{H_w}}} \quad (3.1.2\text{-}10)$$

$$\mathrm{C_D} = 1.9 \times \left(1 + 1.9 \times \frac{\mathrm{b}}{\mathrm{w}} \times \frac{1}{2}\right)^2 \quad (3.1.2\text{-}11)$$

$$\lambda = 0.73 + 1.2 \times \frac{\mathrm{b}}{\mathrm{w}} + 1.1 \times \left(\frac{\mathrm{b}}{\mathrm{w}}\right)^2 \quad (3.1.2\text{-}12)$$

In these equations, ρ denotes the density of the flow, while g is the gravitational acceleration constant. The variable Hw represents the inundation depth, and W is the horizontal length of the wall exposed to the water flow. The velocity of the incoming wave is denoted by v, which is calculated based on the Froude number Fr. The drag coefficient C_D and the empirical coefficient λ are both functions of the blocking fraction b/w, where b is the wall width and w is the total channel width. This blocking ratio is critical in determining the flow regime, as higher values promote the transition from subcritical to choked flow. These parameters collectively govern the distribution and intensity of lateral loads applied by tsunami and flood actions.

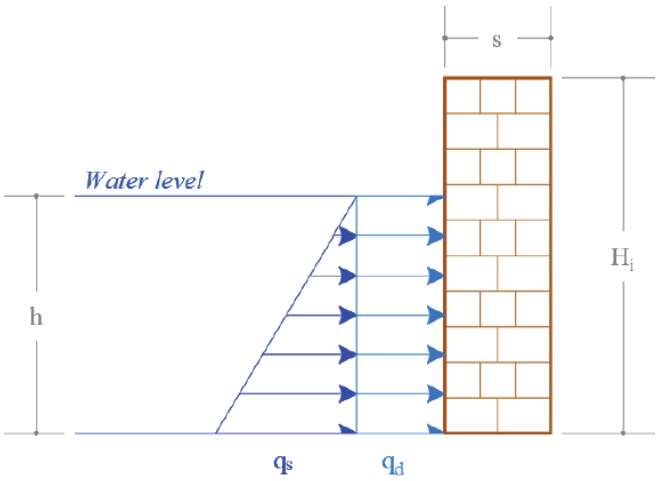

Figure 3.1-3 Tsunami inundation forces model (s is the wall thickness, Hi is the interstorey height, qs is the maximum hydrostatic load, qd is the uniform hydrodynamic load)

The total external work becomes:

$$L_E = R_1 \times h_1 \times \varphi \ + R_2 \times h_2 \times \varphi \tag{3.1.2-13}$$

This collapse verification under tsunami-induced loading conditions still follows the same virtual work principle outlined in Equation (3.6), where internal work is balanced against the external work contributions from lateral (tsunami) and axial forces. Despite the different force origins, the governing condition for collapse remains:

$$L_{i,max} = L_E + L_P \tag{3.1.2-14}$$

Thus, the analysis framework for seismic and tsunami scenarios can be unified using this energy-based approach.

3.2. Flexural Design of Strengthened Masonry Walls

This section presents the theoretical background and design procedure for both FRP- and FRCM-strengthened walls, based on the respective Italian code provisions. An illustrative design example is shown in Figure 3.2-1 to clarify the calculation procedure.

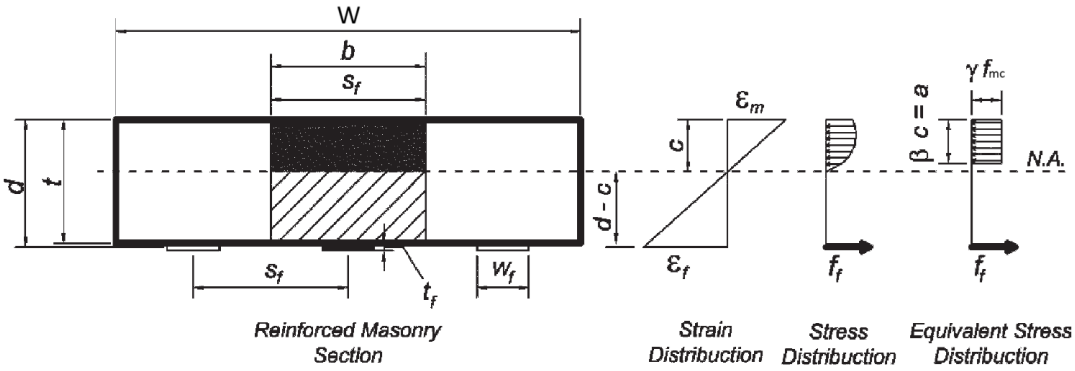

Figure 3.2-1 URM walls strengthened with FRP or FRCM.

3.2.1. FRP Strengthening

The design strain of FRP is:

$$\varepsilon_{fd} = min\left\{\eta \times \frac{\varepsilon_{fk}}{\gamma_f}, \varepsilon_{fdd}\right\} \quad (3.2.1\text{-}1)$$

Where ε_{fk} is the characteristic ultimate strain of the fiber, ε_{fdd} is the maximum design strain in FRP due to end debonding, γ_f is the partial safety factor see Table 3-1 , and $\eta = \eta_a \times \eta_l$ accounts for environmental and long-term effects, see Table 3-2 and

Table ***3-3*** . This formulation ensures a conservative design by considering both rupture and debonding risks. Table 3-1 provides recommended values for γ_f based on material type and safety level, while Table 3-2 and

Table ***3-3*** specifies the environmental reduction factor η_a and η_l for different exposure conditions.

These formulations are based on the provisions of CNR-DT 200 [35], specifically pages 34–37 and page 64, which ensure a conservative design by considering both rupture and debonding risks.

Table 3-1 Partial factors γ_f.

Limit State		
SLE	γ_{f0}	1.00
SLU: Tensile failure of FRP laminates	γ_{f1}	1.25
SLU: Tensile failure of in-situ impregnated fabrics	γ_{f1}	1.30
SLU: Detachment from the substrate for EBR systems	γ_{f2}	1.30
SLU: Detachment from the substrate for EBR systems with cord anchors	γ_{f2}	1.30
SLU: Detachment from the substrate for NSM systems:	γ_{f3}	
NSM with rough, deformed, or spirally wrapped surfaces		1.30
NSM with smooth laminates and bars or with resin-sand finished surfaces		1.70

Table 3-2 Environmental conversion factor η_a for various exposure conditions and FRP systems with an epoxy resin matrix.

Exposure Condition	Type of Fiber	η_a
Indoor	Glass	0.75
	Aramid	0.85
	Carbon – Preformed	0.95
	Carbon – Prepreg and in-situ impregnated	0.95
	Steel	0.95
Outdoor	Glass	0.65
	Aramid	0.75
	Carbon – Preformed	0.95
	Carbon – Prepreg and in-situ impregnated	0.80
	Steel	0.80
Aggressive Environment	Glass	0.50
	Aramid	0.70
	Carbon – Preformed	0.90
	Carbon – Prepreg and in-situ impregnated	0.75
	Steel	0.75

Table 3-3 Environmental conversion factor η_l a for various exposure conditions and FRP systems with an epoxy resin matrix.

Loading mode	Type of fiber / matrix	η_l (SLS)	η_l (ULS)
Quasi-permanent and/or cyclic (creep, relaxation and fatigue)	Glass / Vinylesters or epoxy	0.30	1.00
	Aramid / Vinylesters or epoxy	0.50	1.00
	Carbon / Vinylesters or epoxy	0.90	1.00

The maximum design stress related to end debonding is given by the provisions of CNR-DT 200 [28], specifically pages 42–43. This approach ensures a conservative design by accounting for both rupture and debonding risks.

$$f_{fdd} = \frac{k_b}{\gamma_{f2}} \times \sqrt{\frac{2 \times E_f \times \Gamma_{Fk}}{t_f}} \tag{3.2.1-2}$$

Where γ_{f2} is the partial factor equal to 1.3 for ULS of detachment from the support.

The geometric coefficient k_b is:

$$k_b = \sqrt{\frac{2 - \frac{w_f}{w}}{1 + \frac{w_f}{w}}} \tag{3.2.1-3}$$

Γ_{Fk} is the characteristic value of the maximum bond stress at the FRP-masonry interface and is calculated as:

$$f_{bk} = k_{Gk} \times \frac{\sqrt{f_{cm} \times f_{ctm}}}{2 \times FC} \tag{3.2.1-4}$$

$$\Gamma_{Fk} = \frac{1}{2} \times f_{bk} \times s_u \tag{3.2.1-5}$$

With $k_{Gk} = 0.15$ for brick masonry, FC=1, and$s_u = 0.4$mm.The strain ε_{fdd} is then obtained as:

$$\varepsilon_{fdd} = \frac{f_{fdd}}{E_f} \quad (3.2.1\text{-}6)$$

The coefficient k_{Gk} provided in Table 3.4 is based on the provisions of CNR-DT 200 [28], specifically page 113, and represents the characteristic value of the dimensionless factor calibrated through experimental data in accordance with EN 1990.

Table 3-4 Characteristic value.

Brick masonry	0.15
Tuff masonry	0.6
Sicilian calcarenite masonry	0.38
Lecce stone masonry	0.12

The ultimate , s_u, of the bond interface, as used in Equation 3-21, is differentiated based on the type of masonry substrate (see Table 3.5), which is based on the provisions of CNR-DT 200 [28], specifically page 111.

Table 3-5 Ultimate slip.

Brick masonry	0.4mm
Campanian tuff blocks	0.4mm
Sicilian calcarenite masonry	0.3mm
Lecce stone masonry	0.3mm

This conservative definition allows the design to avoid failure at the interface without the need for direct bond test data.

The following formulas, including the calculation of the design stress, effective reinforcement area, reinforcement ratio, balanced reinforcement ratio, and ultimate moment capacity, are based on the analytical framework provided by Galati et al. in SP-230—16 Design Guidelines for Masonry Structures: Out-of-Plane Loads [43]. While the conceptual approach follows the recommendations of CNR-DT 200 [35], specifically in defining the material safety factors, reduction coefficients, and failure modes, it is important to note that CNR-DT 200 does not provide a complete set of explicit equations or worked design examples for FRP-strengthened

masonry walls. CNR-DT 200 serves as a guideline document rather than a detailed design manual. Therefore, the detailed formulations and calculation steps employed herein are referenced from [43] to ensure a comprehensive and practical design methodology, while maintaining full consistency with the principles and safety philosophy outlined in CNR-DT 200.

The corresponding design stress is:

$$f_{fd} = \varepsilon_{fd} \times E_f \tag{3.2.1-7}$$

Where E_f is the elastic modulus of the FRP.

The effective reinforcement area is:

$$A_f = W \times \frac{w_f}{s_f} \times t_f \times n_l \tag{3.2.1-8}$$

With W as the wall sidth, w_f as the FRP width, s_f as the FRP spacing, t_f thickness of the fiber, n_l and the number of layers.

The reinforcement ratio is:

$$\rho_f = \frac{n_s \times A_f}{W \times t} \tag{3.2.1-9}$$

Where n_s is the number of FRP, W is the wall width, and t is the wall thickness.

The balanced reinforcement ratio defines the transition point between failure governed by masonry crushing and that governed by FRP rupture or debonding. It is evaluated as:

$$\rho_{fb} = \frac{f_{mc}}{f_{fd}} \times [\gamma \times \beta \times \frac{\varepsilon_{mu}}{\varepsilon_{mu} + \varepsilon_{fd}} - \frac{P}{W \times t \times f_{mc}}] \tag{3.2.1-10}$$

- If $\rho_f > \rho_{fb}$, masonry crushing governs, and the moment capacity is:

$$M_n = \gamma \times f_{mc} \times a \times W \times \left(d - \frac{a}{2}\right) - P \times \left(d - \frac{t}{2}\right)$$

$$= n_s \times A_f \times f_f \times \left(d - \frac{a}{2}\right) + P \times \left(\frac{t}{2} - \frac{a}{2}\right) \tag{3.2.1-11}$$

$$f_f = E_f \times \varepsilon_{mu} \times \frac{\beta \times d - a}{a} \tag{3.2.1-12}$$

$$a = \beta \times c = \frac{(n_s \times A_f \times f_f + P)}{\gamma \times f_{mc} \times W} \tag{3.2.1-13}$$

- If $\rho_f < \rho_{fb}$, rupture or debonding governs:

$$M_n = 0.8 \times f_{mc} \times 0.8 \times c \times W \times \left(d - \frac{0.8 \times c}{2}\right) - P \times \left(d - \frac{t}{2}\right)$$

$$= n_s \times A_f \times f_f \times \left(d - \frac{0.8 \times c}{2}\right) + P \times \left(\frac{t}{2} - \frac{0.8 \times c}{2}\right) \tag{3.2.1-14}$$

$$f_f = E_f \times \varepsilon_{mu} \times \frac{d-c}{c} \leq f_{fd} \quad (3.2.1\text{-}15)$$

$$c = \frac{\rho_f \times t}{0.8^2 \times f_{mc}} \times \left[\sqrt{\left(\frac{E_f \times \varepsilon_{mu}}{2} - \frac{P}{2 \times n_s \times A_f} \right)^2 + \frac{0.8^2 \times f_{mc} \times d \times E_f \times \varepsilon_{mu}}{\rho_f \times t}} - \left(\frac{E_f \times \varepsilon_{mu}}{2} - \frac{P}{2 \times n_s \times A_f} \right) \right] \quad (3.2.1\text{-}16)$$

Where a is compression block depth and c is neutral axis depth.

3.2.2. FRCM Strengthening

The strengthening of masonry walls using Fabric-Reinforced Cementitious Matrix (FRCM) systems is an effective solution for improving out-of-plane performance, particularly under combined axial and bending loads. This section presents a detailed design methodology strictly following the procedure exemplified in Section 11.2 of CNR-DT 215/2018 [36]. Unlike CNR-DT 200 [35], which does not provide explicit design formulas or worked examples for FRP-strengthened masonry walls, CNR-DT 215 offers a complete step-by-step calculation example for FRCM-strengthened walls in Section 11.2. The approach integrates the identification of potential failure modes directly into the calculation process, using formula-based verification to distinguish between masonry crushing and FRCM rupture or debonding. For each case, the neutral axis position, internal force equilibrium, flexural capacity, and verification of the failure assumption are systematically addressed.

In practice, the mechanical properties usually provided by FRCM manufacturers are limited to the elastic modulus of the dry fabric, the characteristic value of the ultimate stress of the dry fabric, and the characteristic value of the ultimate strain of the dry fabric. If additional data, such as the characteristic value of the ultimate stress of the FRCM strengthening, the average ultimate strain, or the debonding capacity are not provided by the supplier or the corresponding European Technical Assessment (ETA) documents,it is recommended to estimate these parameters based on reference values from the literature. The suggested reference values and estimation methods are summarized in Table 3-6.

Table 3-6 Estimated mechanical parameters of FRCM systems based on literature.

Parameter	Estimation Method	Typical Ratio	Description
Ultimate stress of FRCM σ_u	$\sigma_u = k \times \sigma_{u,f}$		The tensile strength of the FRCM system is approximately

		approx. 80%–100%	80%–100% of the dry fabric strength; some tests even show higher values [44].
Ultimate strain of FRCM ε_u	$\varepsilon_u = k \times \varepsilon_{u,f}$	approx. 80%–100%	The ultimate strain of the FRCM system is generally close to that of the dry fabric, typically in the 80%–100% range [44].
Debonding stress $\sigma_{lim,conv}$	$\sigma_{lim,conv} = k \times \sigma_{u,f}$	approx. 60%–80%	Literature indicates that the debonding strength of steel-FRCM systems is typically 60%–80% of the dry fabric strength [45].
Debonding strain $\varepsilon_{lim,conv}$	$\varepsilon_{\mathrm{lim,conv}} = \sigma_{lim,conv}/E_f$	Calculated directly	The debonding strain is calculated directly from the debonding stress and the elastic modulus of the dry fabric without additional empirical factors.

The design strain of the FRCM, ε_{fd}, is calculated by considering both environmental conditions and material properties. It is defined as:

$$\varepsilon_{fd} = min\left\{\eta_a \times \frac{\alpha \times \varepsilon_{lim,conv}}{\gamma_m}, \eta_a \times \frac{\varepsilon_u}{\gamma_m}\right\} \quad (3.2.2\text{-}1)$$

where α is the amplification coefficient, typically 1.5, $\varepsilon_{\mathrm{lim,conv}}$ is the conventional strain limit, ε_{u} is the average value of the ultimate strain of the FRCM strengthening,γ_{m} is the material partial safety factor, and η_{a} is the environmental reduction factor see Table 3-7.

As illustrated in Figure 3.2-2, the typical tensile behavior of FRCM systems obtained from direct tensile tests presents an initial linear elastic phase controlled by the dry fabric modulus E_f, followed by a nonlinear cracked stage, and finally reaches either the debonding strain limit $\varepsilon_{lim,conv}$ or the ultimate strain ε_u. The corresponding stress-strain curve clearly shows these key points along with the effects of the amplification coefficient α used in the design strain calculation.

Although the tensile strength of FRCM systems shown in the figure appears higher than that of the dry fabric, it is essential to adopt conservative values in design. This is because actual FRCM performance can be influenced by factors such as workmanship, bond quality, and environmental conditions, which introduce uncertainties. Therefore, design guidelines recommend using characteristic values based on approximately 80%–100% of the dry fabric properties to avoid overestimation.

MDPI (Gattesco et al., 2021) [45] indicated that in some cases, the peak tensile strength of a well-bonded Steel-FRCM system could reach 105%–120% of the dry fabric strength. Similarly, Figure 3.2-2 from CNR-DT 215/2018 also reflects that FRCM systems may exhibit higher peak strength compared to dry fabric alone. Nevertheless, for practical design, the more conservative 80%–100% range is preferred.

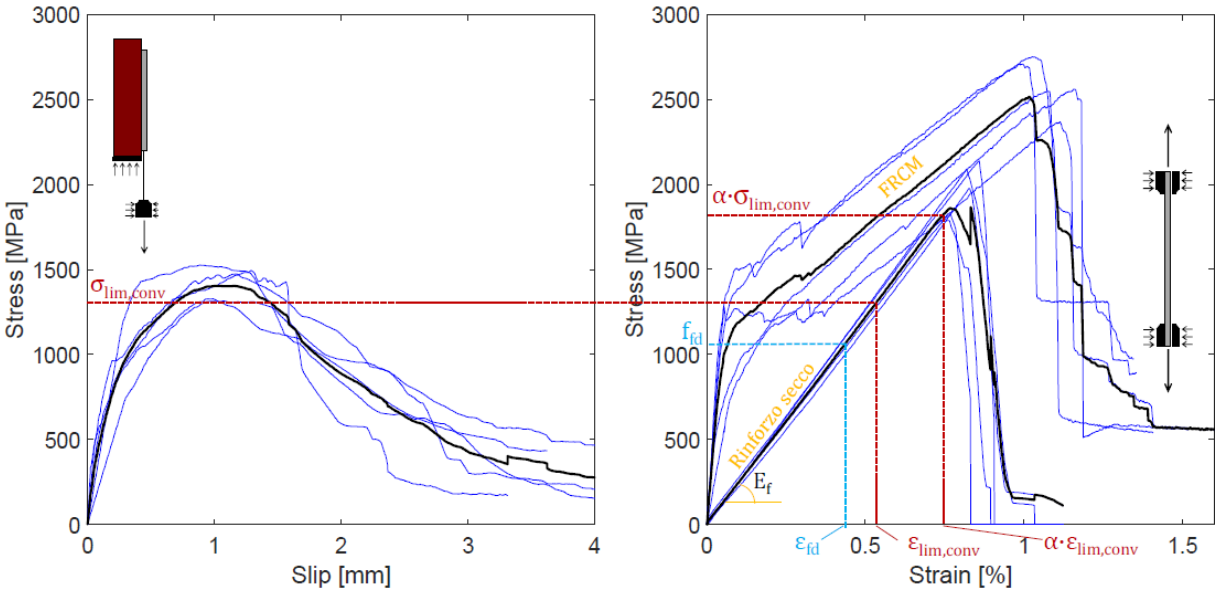

Figure 3.2-2 Average stress-strain curve obtained from direct tensile tests on samples of FRCM.

The design compressive strength of masonry, f_{md}, is calculated as follows:

$$f_{md} = \frac{f_m}{FC \times \gamma_M} \tag{3.2.2-2}$$

where f_m is the characteristic compressive strength of the masonry, γ_M is the partial safety factor for masonry materials, and FC is the confidence factor related to the Level of Knowledge (e.g., LC2 → FC = 1.2).

. **Table 3-7** Environmental conversion factors.

Exposure conditions	η_a
Internal	0.90
External	0.80
Aggressive environment	0.70

In accordance with the methodology prescribed by CNR-DT 215/2018, the flexural capacity of FRCM-retrofitted masonry walls is determined by calculating both possible moment capacities: one corresponding to masonry crushing and the other to FRCM rupture or debonding. Each capacity is computed based on its respective failure strain and mechanical properties.

The governing failure mode is identified by selecting the lower of the two moment capacities, which indicates the critical limit state that will be reached first under loading.

Depending on the identified failure mode, the tensile force in the FRCM, the compressive force in the masonry, and the preliminary neutral axis depth are each calculated using their respective formulas. These distinct formulations ensure that the mechanical behavior of both the FRCM system and the masonry substrate is properly captured for each potential failure mechanism.

- If masonry crushing governs:

$$c = \frac{-\left(E_f \times \varepsilon_{mu} \times n_l \times t_f - P + \sqrt{\left(E_f \times \varepsilon_{mu} \times n_l \times t_f - P\right)^2 + 4 \times 0.85 \times f_{md} \times 0.7 \times E_f \times \varepsilon_{mu} \times n_l \times t_f \times t}\right)}{2 \times 0.85 \times f_{md} \times 0.7} \quad (3.2.2\text{-}3)$$

$$F_m = 0.85 \times f_{md} \times 0.7 \times c \quad (3.2.2\text{-}4)$$

$$F_f = E_f \times \frac{\varepsilon_{mu}}{c} \times (t - c) \times n_l \times t_f \quad (3.2.2\text{-}5)$$

- If FRCM rupture or detachment governs:

$$c = \frac{E_f \times \varepsilon_{fd} \times n_l \times t_f + P}{0.85 \times f_{md} \times 0.7} \quad (3.2.2\text{-}6)$$

$$F_m = 0.85 \times f_{md} \times 0.7 \times c \quad (3.2.2\text{-}7)$$

$$F_f = E_f \times \varepsilon_{fd} \times n_l \times t_f \quad (3.2.2\text{-}8)$$

In these calculations, n_l represents the number of FRCM reinforcement layers applied to the masonry wall, while c denotes the neutral axis depth associated with the internal force equilibrium. The term F_m corresponds to the compressive force developed within the masonry, whereas F_f refers to the tensile force carried by the FRCM system. The parameter t_f indicates

the thickness of the FRCM reinforcement, and P represents the external axial load acting on the wall.

Regardless of whether masonry crushing or FRCM rupture governs the failure, the subsequent flexural capacity calculation follows the same procedure. The calculation formulas for the flexural capacity M_R and the final design moment M_{Rd} are given as follows. Additionally, for unstrengthened masonry walls, the corresponding moment capacity is denoted as M_R^{UR}, which serves as the baseline for evaluating the improvement provided by strengthening interventions.

$$M_R^{UR} = P \times \left(\frac{t}{2} - \frac{\beta \times c}{2}\right) \quad (3.2.2\text{-}9)$$

$$M_R = W \times \left(F_m \times \left(\frac{t}{2} - \frac{0.7 \times c}{2}\right) + F_f \times \frac{t}{2}\right) \quad (3.2.2\text{-}10)$$

$$M_{Rd} = M_R^{UR} + \frac{1}{\gamma_{Rd}} \times (M_R - M_R^{UR}) \quad (3.2.2\text{-}11)$$

Where γ_{Rd} represents the global safety factor typically adopted as 2 for conservative design purposes.

3.3. Numerical Implementation for Strengthened and Unstrengthened Masonry Walls under Seismic and Tsunami Loading

A numerical simulation framework was developed using MATLAB to assess the structural performance of masonry walls under extreme loading conditions. This framework uses the principle of virtual work and includes models for both unstrengthened and retrofitted walls.

Three strengthening conditions are considered: no reinforcement, externally bonded FRP, and FRCM grid systems. Each configuration is analyzed under two distinct loading scenarios—seismic and tsunami—representing lateral loading mechanisms with different characteristics.

The objective of this numerical implementation is to calculate the moment capacity for each wall configuration and loading condition and then use it to back-calculate the corresponding external actions that may cause failure.

In the seismic loading scenario, the moment capacity is used to reverse-engineer the equivalent lateral force through the virtual work principle.

For tsunami loading, the model uses the computed moment capacity to estimate the resulting force and the floodwater height required to trigger collapse.

This section presents the development of the computational model and its application across all six scenarios, combining three wall configurations (unstrengthened, FRP-strengthened, and FRCM-strengthened) with two hazard types (seismic and tsunami).

3.3.1. Numerical Model for Unstrengthened Masonry Walls under Seismic and Tsunami Loading

To establish a benchmark for comparison, this section simulates the behavior of unstrengthened masonry walls subjected to both seismic and tsunami loading using the principle of virtual work. For the seismic scenario, a pair of concentrated lateral loads is applied at two specific points along the wall height to simulate the effect of inertial forces induced by seismic excitation, as depicted in Figure 3.1-1. In contrast, the tsunami scenario involves a distributed hydrostatic and hydrodynamic pressure profile acting along the wall height, as shown in Figure 3.1-2

The MATLAB code computes the critical rotation angle that leads to collapse and derives the equivalent lateral force and displacement under each loading condition. The wall is modeled as a single-layer homogeneous element with axial compression and no additional reinforcement. Material properties such as compressive strength and elastic modulus are based on experimental reference values.

In the early phase of analysis, force-displacement diagrams were also derived using Excel by discretizing the virtual work equilibrium equations. While Excel provides a useful environment for preliminary modeling of unstrengthened walls, the complexity of strengthened wall scenarios—particularly those involving multiple failure modes and composite interactions—necessitates the use of MATLAB due to its higher computational flexibility and automation capabilities.

These results provide baseline data for comparing the performance of FRP and FRCM retrofitted walls under multi-hazard scenarios.

3.3.2. Implementation for FRP-Strengthened Masonry Walls under Seismic and Tsunami Loading

To evaluate the influence of FRP strengthening on the out-of-plane response of masonry walls, this section presents the numerical implementation of the virtual work model for walls retrofitted using externally bonded Fiber-Reinforced Polymer (FRP) strips. The simulation covers both seismic and tsunami loading scenarios.

Material and design parameters are defined in accordance with the CNR-DT 200 R2/2025 guideline, which prescribes a conservative design strain calculated as the minimum between the rupture strain and the end debonding strain of the FRP. This ensures safety by limiting the overestimation of the system’s flexural capacity.

In the MATLAB implementation, the governing failure mode—either masonry crushing or FRP rupture/debonding—is determined automatically by comparing the actual reinforcement ratio ρ_f with the balanced reinforcement ratio ρ_{fb}.Once the failure mode is identified, the corresponding design strain is used to calculate the initial moment capacity.

After obtaining the moment capacity, the critical moment is used in reverse through the virtual work equations to estimate the maximum equivalent external action.

For seismic loading, this corresponds to the equivalent lateral force required to cause out-of-plane collapse.

For tsunami loading, the calculated moment is used to estimate both the equivalent force and the required floodwater height that could lead to failure.

These results provide valuable insights into the effectiveness of FRP retrofitting under different hazard scenarios and contribute to a comprehensive assessment of both seismic and tsunami resilience.

3.3.3. Implementation for FRCM-Strengthened Masonry Walls under Seismic and Tsunami Loading

This section extends the numerical model to simulate masonry walls retrofitted with FRCM (Fabric-Reinforced Cementitious Matrix) systems. The modeling procedure follows the same structure used for the FRP-strengthened case but adopts material-specific parameters and failure conditions based on CNR-DT 215/2018.

The design strain is conservatively defined as the minimum between the rupture strain of the dry textile and the matrix debonding strain, reduced by environmental and long-term effects through the factor and divided by a fixed partial safety factor. This formulation ensures safety and consistency in flexural design.

In the MATLAB implementation, the governing failure mode is determined in accordance with the procedure prescribed by CNR-DT 215:2018. Specifically, the moment capacities associated with masonry crushing and with FRCM rupture or debonding are both computed using their respective design formulations. The smaller of these two moment capacities is identified as the critical value, as it represents the limit state that will be reached first.

This methodology offers a rational and code-compliant framework for identifying the controlling failure mechanism and ensures consistency with established design practice.

After calculating the moment capacities corresponding to masonry crushing and FRCM rupture or debonding, the smaller value is identified as the governing capacity. This critical moment is

subsequently utilized in reverse, applying the principle of virtual work to estimate the maximum equivalent external action.

In the case of seismic loading, the critical moment is used to reverse the equivalent lateral force necessary to induce out-of-plane collapse. For tsunami loading, the selected moment capacity is employed to back-calculate both the equivalent horizontal force and the corresponding floodwater height required to reach the failure condition.

This section presents the computational implementation of the proposed methodology for all FRCM-retrofitted masonry walls under multi-hazard scenarios and establishes a consistent basis for comparison with unstrengthened and FRP-retrofitted configurations, which are discussed in Chapter 4.

3.3.4. MATLAB Simulation of Unstrengthened and Strengthened Masonry Walls under Seismic and Tsunami Actions

After defining the governing equations and implementing the relevant material and geometric parameters, six separate MATLAB scripts were developed—each corresponding to a specific strengthening condition and loading scenario. These simulations cover all possible combinations of wall types (unstrengthened, FRP-strengthened, and FRCM-strengthened) and hazard types (seismic and tsunami), as summarized below:

1. Unstrengthened masonry wall under seismic loading.
2. Unstrengthened masonry wall under tsunami loading.
3. FRP-strengthened wall under seismic loading.
4. FRP-strengthened wall under tsunami loading.
5. FRCM-strengthened wall under seismic loading.
6. FRCM-strengthened wall under tsunami loading.

For each case, the MATLAB implementation outputs:

1. For unstrengthened masonry walls, the MATLAB model generates force-displacement curves under both seismic and tsunami loading conditions to facilitate comparison with experimental results.
2. Governing failure mode (masonry crushing, FRP/FRCM rupture, or FRP/FRCM debonding).
3. Maximum moment capacity (Mn).
4. Maximum out-of-plane loads, or flood height.

These results allow for a comprehensive comparison of retrofitting strategies under both seismic and tsunami hazards and form the analytical basis for discussion in Chapter 5.

THIS PAGE WAS INTENTIONALLY LEFT BLANK

4. NUMERICAL MODELLING AND MATLAB IMPLEMENTATION

4.1. Introduction

This chapter presents the development of a numerical modeling framework implemented in MATLAB to simulate the out-of-plane (OOP) behavior of unreinforced masonry (URM) walls under seismic and tsunami-induced loading, both before and after retrofitting with composite strengthening systems (FRP and FRCM). The goal is to translate the theoretical models introduced in Chapter 3 into an automated computational environment that allows for efficient parametric studies and practical applications.

The proposed MATLAB framework is designed to:

1. Compute moment capacities for unstrengthened and strengthened masonry walls.
2. Reverse-engineer equivalent external forces using the principle of virtual work.
3. Identify governing failure modes (masonry crushing vs. reinforcement rupture or debonding).
4. Validate results against experimental data and design standards.

4.2.Overview of the Numerical Modeling Framework

4.2.1. Phase 1: Input Definition

The following parameters are required as inputs:

1 Wall Geometry: including wall height, wall width, and wall thickness.

2 Material Properties:

- 2.1 For masonry, the required properties include compressive strength and elastic modulus.
- 2.2 For FRP or FRCM systems, the required properties include elastic modulus, design strain, fiber thickness, fiber width, and number of reinforcement layers.

3 Loading Type: Seismic or Tsunami.

4 Axial Load: Vertical compression.

4.2.2. Phase 2: Capacity Calculation

For each wall configuration:

1 Calculate moment capacities according to relevant design codes:
  1.1 Unstrengthened walls: Governed by masonry crushing.
  1.2 FRP strengthening: Based on CNR-DT 200/2025 design strain and failure modes.
  1.3 FRCM strengthening: Based on CNR-DT 215/2018 design strain and failure modes.
2 Compute reinforcement ratios, stress-strain limits, and neutral axis depths.

4.2.3. Phase 3: Virtual Work and Reverse Analysis

For unstrengthened masonry walls, the collapse loads are estimated by applying the principle of virtual work, which allows for the calculation of equivalent lateral forces and displacement in seismic loading scenarios or critical flood height and maximum hydrodynamic forces in tsunami loading scenarios. Full force-displacement curves are generated for these unstrengthened configurations to support detailed behavioral assessment.

For FRP-retrofitted masonry walls, the failure mode is determined in advance by comparing the reinforcement ratio, denoted as ρ_f, with the balanced reinforcement ratio, denoted as ρ_{fb}. If the actual reinforcement ratio exceeds the balanced ratio $\rho_f > \rho_{fb}$, masonry crushing is identified as the governing failure mode. Otherwise, failure is governed by FRP rupture or debonding. Once the failure mode is determined, the design moment ,Mn,is calculated, and the principle of virtual work is applied in reverse to derive the maximum equivalent external action. This action may correspond to the maximum lateral force in seismic loading or the critical flood height in tsunami loading. For FRP-strengthened walls, only maximum capacities are provided without generating force-displacement curves.

For FRCM-retrofitted masonry walls, both possible failure modes—masonry crushing and FRCM rupture/detachment—are explicitly calculated following the methodology in CNR-DT 215/2018. The respective moment capacities for each mode are computed, and the governing failure mode is selected as the one yielding the lower capacity. Based on the identified failure mode, the design moment ,Mn, is used to back-calculate the maximum external force using the virtual work principle. Similar to FRP cases, no force-displacement curves are generated for FRCM-retrofitted walls; only the maximum capacities and failure modes are provided for design verification.

This approach ensures a consistent methodology for both FRP and FRCM systems while maintaining clarity in failure mode determination and practical relevance in design applications.

4.3. MATLAB Implementation Structure

The MATLAB numerical model developed in this study was designed to provide a flexible, modular, and efficient tool for evaluating the out-of-plane behavior of masonry walls under multi-hazard loading conditions. The computational structure is divided into distinct modules, each responsible for a specific task, ensuring both clarity and adaptability.

4.3.1. Automatic Failure Mode Identification

For retrofitted walls, the MATLAB code automatically determines the governing failure mode by comparing the calculated strains against design strain limits. This prevents manual errors and ensures that the design follows the most critical failure condition as prescribed by design codes.

4.3.2. Slenderness Verification

The code includes an embedded check of the wall's slenderness ratio (h/t). If the geometry falls below the minimum threshold ($h/t < 15$), a warning message is displayed. Although the analysis can still proceed, the user is notified that the results may not reflect realistic arching behavior. This safeguard enhances model reliability and guides users to assess boundary conditions appropriately.

4.3.3. Modular Structure for Unstrengthened and Retrofitted Walls

The computational model is currently organized into separate calculation modules, each dedicated to a specific wall configuration and loading scenario. The model consists of three main modules:

1. Module A focuses on the calculation of unstrengthened masonry walls under seismic and tsunami loading.
2. Module B handles the analysis of FRP-retrofitted walls based on the design procedures specified in CNR-DT 200.

3. Module C addresses FRCM-retrofitted walls following the guidelines provided in CNR-DT 215.

At present, each module is implemented as an independent MATLAB script without the use of shared subfunctions. The scripts for unstrengthened, FRP-strengthened, and FRCM-strengthened walls have been developed separately, with limited reuse of common computational routines such as moment capacity calculation, virtual work application, and failure mode determination.

While this approach helps maintain clarity and allows each script to focus on its specific calculation logic, it also leads to redundancy and reduced efficiency in code maintenance and future extensions. The lack of shared functions prevents seamless integration of new materials or additional hazard scenarios. Future improvements should focus on developing a more modular and centralized code structure, where common tasks are standardized into shared functions to enhance scalability, consistency, and maintainability.

4.3.4. Output and Result Visualization

The MATLAB implementation developed in this study provides distinct outputs for each combination of wall type and loading scenario, ensuring comprehensive structural assessment. For unstrengthened masonry walls, the seismic scenario yields complete force-displacement curves, allowing for detailed evaluation of stiffness, ultimate lateral capacity, and displacement at collapse. Similarly, under tsunami loading, the model generates full force-displacement responses along with the corresponding critical flood height and maximum horizontal forces (R1, R2), as well as the displacement associated with structural failure. This comprehensive visualization facilitates the understanding of the wall's behavior throughout the loading process.

In contrast, for retrofitted walls, including both FRP- and FRCM-strengthened configurations, the output focuses solely on the maximum capacity without generating full displacement curves. For seismic loading, the model calculates the maximum design moment (Mn), derives the corresponding maximum lateral force, and identifies the governing failure mode—either rupture, debonding, or masonry crushing. For tsunami loading, the outputs consist of the computed design moment, the critical flood height required to reach failure, the maximum horizontal force, and the associated failure mechanism. Since retrofitted walls are designed primarily to enhance peak capacity rather than deformability, no force-displacement curves are produced in these cases. The focus is placed on key design parameters essential for performance verification and comparative analysis.

This output structure ensures that results are presented in a clear and practical format, tailored to the distinct performance characteristics of both unstrengthened and strengthened walls, while maintaining consistency across seismic and tsunami hazard scenarios.

4.4.Model Limitations

Although the MATLAB-based numerical modeling framework developed in this study provides a practical and efficient tool for evaluating the out-of-plane (OOP) behavior of masonry walls under seismic and tsunami loading, several limitations must be acknowledged:

1. Idealized Material Behavior: The model assumes linear-elastic perfectly plastic behavior for masonry, which does not capture progressive damage, cracking, or nonlinear material behavior. This simplification may limit accuracy in the post-peak range.
2. Simplified Boundary Conditions: The analysis assumes fully fixed boundary conditions at the wall supports, without accounting for potential partial fixity, flexibility, or slip that may exist in real-world construction.
3. Neglect of Dynamic Effects: The virtual work principle applied in this model does not consider time-dependent or dynamic effects, such as seismic amplification, inertia forces, or loading rate sensitivity, which may significantly influence actual wall response during earthquakes or tsunami surges.
4. Single Arching Mechanism Assumption: The model is limited to one-way vertical arch mechanisms and does not account for multi-directional bending, higher-order failure modes, or three-dimensional behaviors.

Due to these inherent simplifications, the proposed framework is best suited for preliminary assessments, conceptual design comparisons, and evaluations of retrofitting strategies. For critical structures or detailed design, complementary advanced numerical modeling (e.g., finite element analysis) or experimental validation is recommended.

4.5. Summary

This chapter presented the development of a numerical modelling framework based on the principle of virtual work and implemented in MATLAB to assess the out-of-plane behaviour of both unreinforced and retrofitted masonry walls subjected to seismic and tsunami-induced loading.

The framework successfully translated theoretical models into an automated computational environment. It enables the calculation of moment capacities, the reverse derivation of equivalent external actions, the automatic identification of failure modes, and the generation of clear and structured output results. Key features such as the integration of slenderness verification and the dual consideration of potential failure modes were emphasized.

Although the model has inherent simplifications, it offers valuable insights for preliminary evaluation of structural performance and for the development of retrofit strategies. The framework provides a practical and adaptable decision-making tool for multi-hazard risk mitigation, while recognizing the need for complementary detailed analysis for critical structures.

The numerical approach and modelling tools developed in this chapter will form the basis for the analysis and comparative evaluation of various case studies presented in Chapter 5. In the following chapter, the proposed model will be applied to assess the effectiveness of different strengthening strategies and to validate the computational results against experimental data, thereby demonstrating its practical relevance and limitations.

5. EVALUATION AND EXPERIMENTAL COMPARISON OF STRENGTHENING STRATEGIES

This chapter presents the results obtained from the numerical simulations described in Chapter 3. The unstrengthened masonry wall was thoroughly analyzed under both seismic and tsunami loading scenarios to establish a baseline. Selected cases of FRP- and FRCM-strengthened walls were also simulated to allow for comparative evaluation, but not all strengthened configurations were included.

For each case, the MATLAB implementation provided essential structural indicators, including moment capacity, failure mode, equivalent lateral force (for seismic loading), and floodwater height and resulting force (for tsunami loading).

The moment capacities were calculated based on the CNR design guidelines, and these values were then used in reverse through the virtual work equations to estimate the corresponding external actions. The reverse-derived results were compared against experimental data to assess the accuracy of the model and the effectiveness of the applied strengthening strategies.

5.1. Validation of the Virtual Work Model through Experimental Comparison

To verify the accuracy of the proposed numerical simulation based on the virtual work principle, the unstrengthened masonry wall model was validated against experimental data under both seismic and tsunami loading scenarios. Two approaches—MATLAB and Excel—were used to implement the theoretical formulation, allowing direct comparison with laboratory-obtained force-displacement responses.

5.1.1. Seismic Loading Comparison

Error! Reference source not found. illustrates the force-displacement behavior under seismic c onditions. Both MATLAB and Excel simulations closely follow the initial ascending stiffness observed in the experiment, with the peak force from MATLAB and Excel estimated at 35.83 kN, which aligns well with the experimental peak of 36.37 kN. The correlation suggests that

the virtual work-based model can accurately capture the ultimate capacity and stiffness of unreinforced masonry walls under lateral seismic excitation.

The geometric and mechanical properties used in the simulation are summarized in Table 5-1. These values are consistent with the experimental setup, ensuring a meaningful comparison. The laboratory test setup used for experimental validation is shown in Figure 5.1-2.

Table 5-1 Wall geometry and material properties for validation cases.

Loading Type	Width (m)	Height (m)	Thickness (m)	f_m (MPa)	E_m (GPa)	Axial Load (KN)
Seismic	1.16	1.16	0.12	3.4	0.5	60

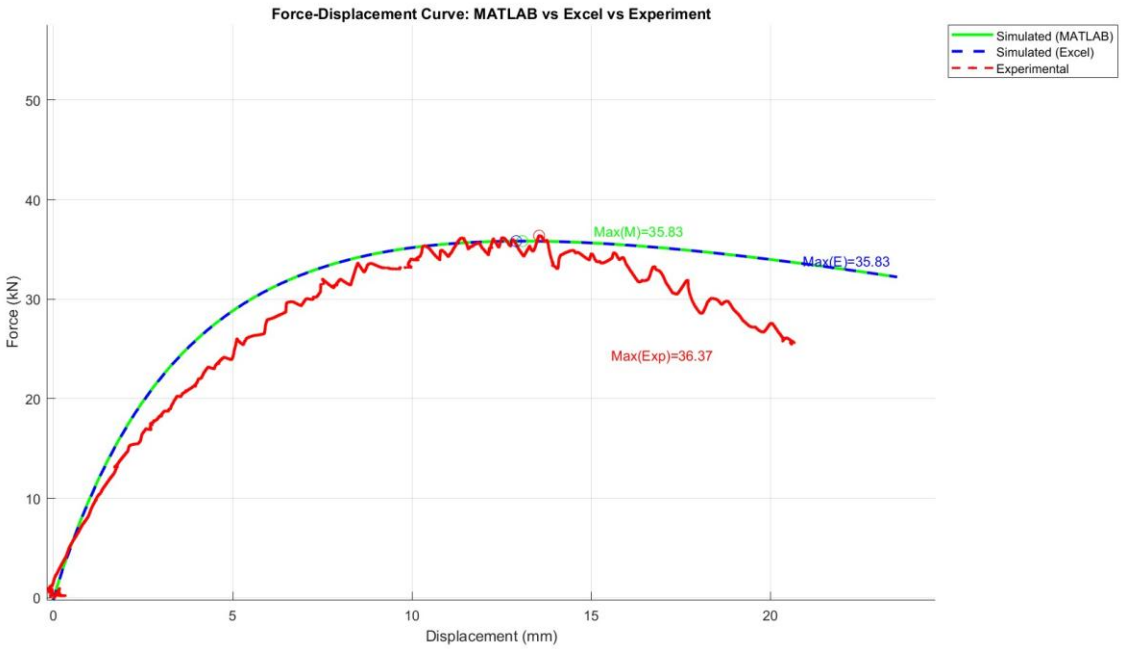

Figure 5.1-1 Force–displacement curve under seismic loading: comparison of MATLAB, Excel, and experimental results.

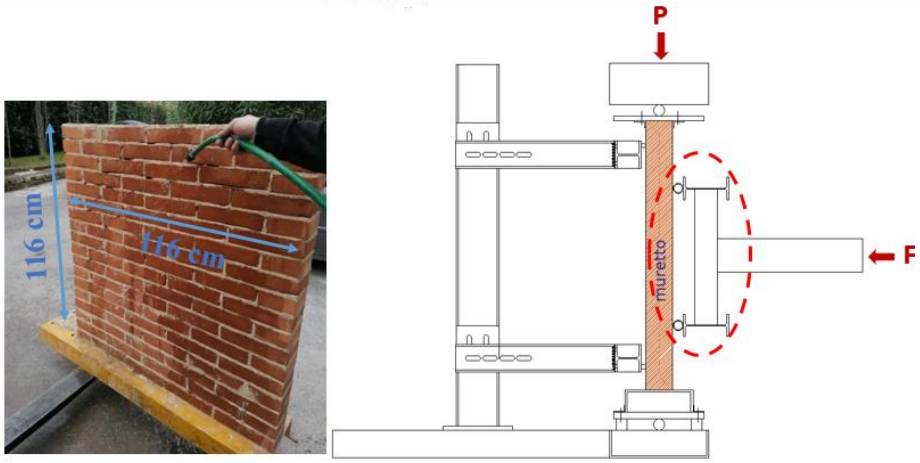

Figure 5.1-2 Experimental setup for seismic out-of-plane test on unreinforced masonry wall.

To validate the proposed theoretical framework, an additional reference was considered for comparison. The wall specimen OOP_2E_AB from reference [46], whose geometric properties are summarized in Table 5-2. It was tested experimentally with a peak load of 9.9 kN. Using the virtual work principle, the predicted maximum lateral force was 10.1 kN, as illustrated in Figure 5.1-3. The close agreement between the theoretical and experimental values confirms that the proposed model offers a reliable approximation of the actual structural behavior.

The laboratory test setup used for experimental validation is shown in

(a) (b)

Figure *5.1-4*.

Table 5-2 Wall geometry and material properties for validation cases.

Loading Type	Width (m)	Height (m)	Thickness (m)	f_m (MPa)	E_m (GPa)	Axial Load (KN)
Seismic	2.35	1.83	0.08	1.81	1.09	0

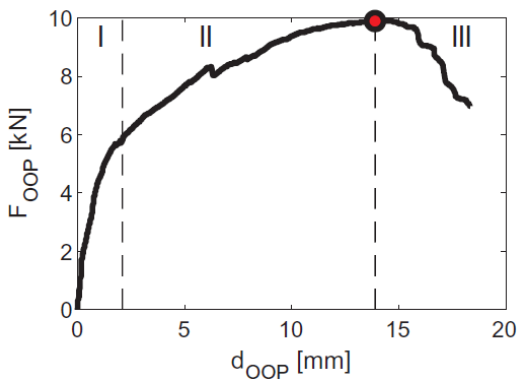

(a)

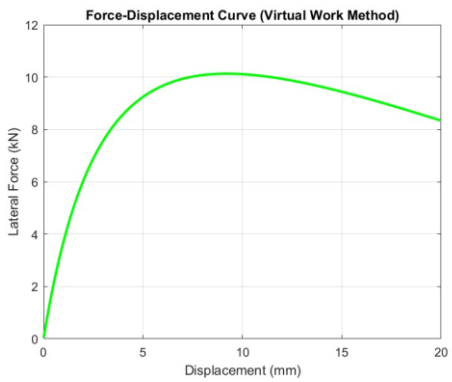

(b)

Figure 5.1-3 Comparison of out-of-plane response for the reference wall specimen and the numerical model: (a) experimental force-displacement curve from [46]; (b) theoretical prediction using the virtual work method.

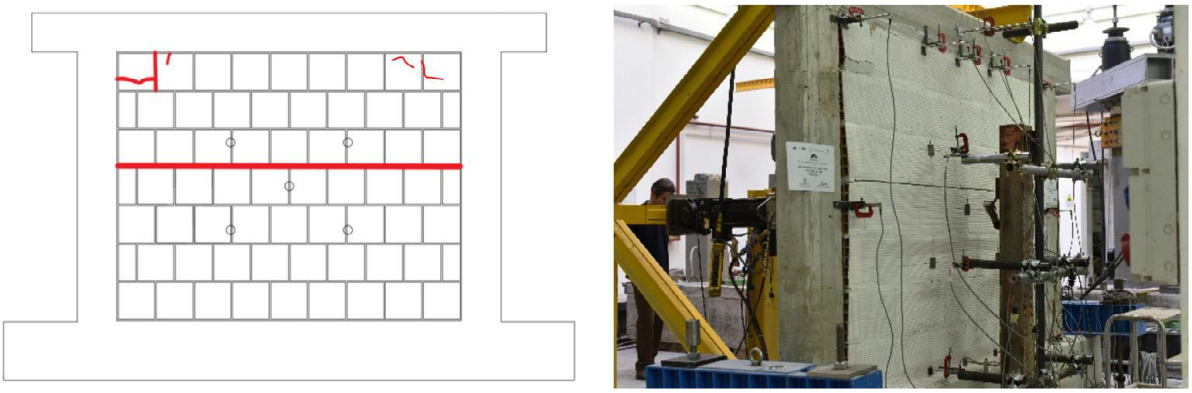

(a) (b)

Figure 5.1-4 Specimen OOP_2E_AB at the end of the test: (a) cracking pattern, (b) photograph.

5.1.2. Tsunami Loading Comparison

Under tsunami-type loading, as the floodwater level rises, the distributed pressure acting on the wall progressively increases until the wall eventually collapse. Figure 5.1-5 presents the relationship between the resulting force R_1 and displacement. The MATLAB model predicted a peak resulting force of 48.35 kN and a corresponding critical flood height of approximately 1.46 m, which closely matches the Excel-derived results of 48.77 kN and 1.47 m. The experimental maximum force was measured at 45.89 kN, associated with an observed flood height of around 1.20 m. The numerical predictions demonstrate acceptable accuracy, particularly in identifying the onset of failure.

The geometric and mechanical properties used in the simulation are summarized in Table 5-3. These values are consistent with the experimental setup, ensuring a meaningful comparison.

The laboratory test setup used for experimental validation is shown in Figure 5.1-6.

Table 5-3 Wall geometry and material properties for validation cases.

Loading Type	Width (m)	Height (m)	Thickness (m)	f_m (MPa)	E_m (GPa)	Axial Load (KN)
Tsunami	4.20	2.30	0.12	3.0	1.2	60

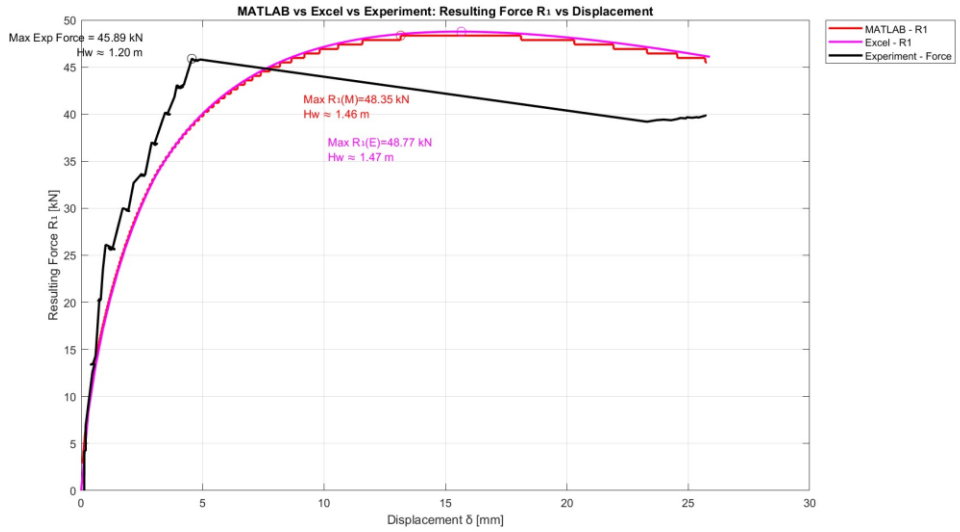

Figure 5.1-5 Resulting force and flood height versus displacement under tsunami loading validation.

(a) (b)

Figure 5.1-6 (a) Experimental setup and (b) failure of unreinforced masonry wall under tsunami loading.

These results confirm that the virtual work-based approach is valid for capturing the out-of-plane capacity of masonry walls in both concentrated (seismic) and distributed (tsunami) loading conditions. The observed deviation post-peak is attributed to nonlinear failure mechanisms and local material degradation not captured by the simplified model.

5.2. Performance Evaluation of Strengthened Masonry Walls

This section presents the out-of-plane performance of masonry walls retrofitted using externally bonded FRP and FRCM systems. Results are derived from the numerical framework based on

the virtual work principle as described in Chapter 3. The objective is to evaluate the improvement in moment capacity, lateral resistance, and flood resilience compared to the unstrengthened baseline cases discussed in Section 5.1.

Each strengthening configuration is analyzed under both seismic and tsunami loading scenarios. The governing failure mode—whether masonry crushing or reinforcement failure—is identified for each case. Comparisons with experimental data are also made to assess the reliability of the model and the effectiveness of the strengthening strategies.

5.2.1. FRP-Strengthened Wall under Seismic Loading

In order to verify the applicability of the theoretical model developed in this thesis, external data from existing literature were referenced. Specifically, experimental data were extracted from the study "Experimental assessment of the out-of-plane response of strengthened one-way spanning masonry infill walls" Verderame et al. [46] .

In this validation, Specimen OOP_2E_FRP from the referenced study was selected due to its similar geometry and GFRP layout. The wall geometry and mechanical properties used in this simulation are presented inTable 5-4, while the GFRP material properties and configuration details are summarized in Table 5-5.

The laboratory test setup used for experimental validation is shown in Figure 5.2-2 and Figure 5.2-3.

Table 5-4 Wall geometry and material properties for validation cases.

Loading Type	Width (m)	Height (m)	Thickness (m)	f_m (MPa)	E_m (GPa)	Axial Load (KN)
Seismic	2.35	1.83	0.08	1.81	1.09	0

Table 5-5 Properties of GFRP [46].

Properties of GFRP	Thickness (mm)	Tensile strength (MPa)	Elastic modulus (GPa)	Ultimate tensile strain (%)
	0.057	1620	42	4

All relevant material and geometric properties of the GFRP and masonry system were input into the MATLAB model. The resulting theoretical response, generated using the virtual work

approach, is depicted in Figure 5.2-1. A comparison between the computed results and the experimental data is provided inTable 5-6 highlighting the consistency or discrepancy between the theoretical prediction and the actual performance observed in testing.

Table 5-6 Comparison between numerical results and reference data.

	Present Study	**Verderame et al. [46]]**
Strength(KN)	46.5	19.1

```
1   clc; clear; close all;
2
3   %% ====================================================================
4   %  PARAMETERS: Geometry, Material Properties, and Safety Factors
5   % ====================================================================
6   % Geometry
7   W = 2.35;            % Wall width [m]
8   H = 1.83;            % Wall height [m]
9   t = 0.08;            % Wall thickness [m]
10  gamma = 0.336;       % Load eccentricity ratio (e/H)
11
12  % Masonry Properties
13  fm = 1.81e6;         % Masonry compressive strength [Pa]
```

```
mmand Window

--- Effective Design Strain Check ---
epsilon_fd (FRP rupture)    = 0.024615
epsilon_fdd (Debonding)     = 0.001612
epsilon_fe  (Controlling)   = 0.001612

=== DESIGN RESULTS ===
Unstrengthened Lateral Force             : 10.84 kN
Unstrengthened Moment                    : 0.71 kN·m

--- Strengthened Design (Controlled by epsilon_fe) ---
Maximum Strengthening Moment Mn (reduced): 3.04 kN·m
Reversed Lateral Force Fe (reduced)      : 46.53 kN
Controlling Failure Mode                 : FRP Rupture or Debonding
```

Figure 5.2-1 MATLAB output for OOP_2E_FRP specimen: design moment, reversed lateral force, and failure mode estimation based on CNR-DT 200 R2/2025.

(a) (b)

Figure 5.2-2 Specimen OOP_2E_FRP: (a) application of the adhesive; (b) application.[46]

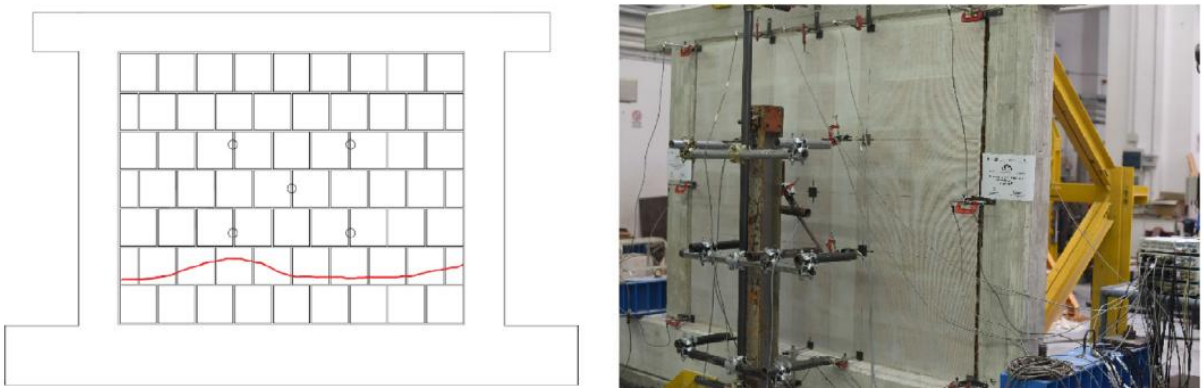

(a) (b)

Figure 5.2-3 Specimen OOP_2E_FRP at the end of the test: (a) cracking pattern, (b) photograph.[46]

The discrepancy between theoretical predictions and experimental outcomes in out-of-plane strengthened masonry walls primarily stems from the limitations inherent in externally bonded CFRP and GFRP systems. Although these materials are widely used in structural retrofitting due to their high tensile strength and ease of installation, experimental results have repeatedly shown that actual performance often falls significantly short of theoretical expectations.

This deviation persists even when design procedures rigorously follow established guidelines and include appropriate safety and reduction factors, as demonstrated by numerous studies that employed international standards such as ACI or CNR but still reported reduced structural capacity in practice [47][48][49].One of the key causes is premature debonding at the fiber–masonry interface, which prevents the full development of the design tensile strain in the fiber- a failure mechanism repeatedly observed in externally bonded FRP systems [47][49]. In many cases, the fiber reinforcement is not fully mobilized due to inadequate adhesion, early cracking

in the substrate, or construction defects. The brittle nature of CFRP and GFRP further contributes to this underperformance, resulting in abrupt strength losses after peak load with limited residual capacity.

Experimental studies have consistently demonstrated that the out-of-plane flexural capacity of URM walls strengthened with FRP systems often falls short of theoretical predictions. For instance, Mosallam [47] investigated CFRP-strengthened clay brick masonry walls subjected to uniformly distributed pressure using a vacuum bag method. Despite strength enhancement compared to unstrengthened specimens, the experimental moment capacity reached only 40% to 60% of the theoretical values, primarily due to premature debonding and localized cracking. Similarly, Griffith et al.[48] conducted full-scale cyclic airbag tests on URM walls retrofitted with GFRP mesh. While these walls demonstrated improved ductility and load resistance, their flexural strength reached only 50% of the predicted capacity, primarily due to mesh slippage, insufficient anchorage, and non-uniform stress distribution. These findings highlight the tendency of conventional FRP design models to overestimate real-world performance, especially when interface behavior and detailing are not adequately considered.

This phenomenon is consistently reported in literature, with experimental capacities of CFRP- or GFRP-strengthened masonry walls typically achieving only 40% to 60% of their theoretical design strength [49][50][51].

This trend is further illustrated in Table 5-7, which summarizes experimental findings across various systems. While externally bonded CFRP and GFRP systems often underperform, FRCM and TRM systems—based on fiber grids embedded in mineral mortars—have shown superior experimental-to-theoretical efficiency, frequently exceeding 85% and in some cases approaching 90% or higher [52][53][54]. These findings underscore the tendency of conventional FRP design approaches to overestimate capacity, highlighting the need for improved modeling of failure mechanisms and bond behavior.

Experimental results further support these observations. In the out-of-plane test of specimen OOP_2E_FRP [46], the first nonlinear behavior was observed at 8.2 kN and 1.7 mm displacement, with a peak load of 19.1 kN at 9.7 mm. A steep post-peak degradation followed, with load reducing to 5.6 kN at 11.8 mm displacement. Cracking and crushing were observed in the masonry infill, while the fiberglass fabric remained intact but partially debonded. This outcome reflects failure driven by substrate crushing and bond loss, rather than fiber rupture, consistent with trends reported in the literature [49][50][51].

Moreover, environmental factors such as poor surface preparation, adhesive curing conditions, humidity, and temperature fluctuations can further undermine FRP effectiveness in real-world applications. In contrast, the mortar-based matrices used in FRCM and TRM systems enable better strain distribution, improved substrate compatibility, and a more progressive failure mode. These advantages lead to greater alignment with theoretical predictions, making them more dependable for practical strengthening scenarios [52][53][54].

Table 5-7 Comparison between theoretical and experimental performance of strengthened masonry walls

Reference	System Type	Theoretical Strength (Design)	Experimental Max. Strength	Experimental Efficiency (%)	Notes
Mosallam[47]	CFRP	100%	40–60%	40–60%	Premature debonding and localized cracking near anchorage
Griffith et al.[48]	GFRP Mesh	100%	50%	50%	Mesh slippage, insufficient anchorage, stress non-uniformity
Valluzzi et al. [49]	CFRP	100%	40–60%	40–60%	Debonding dominates failure behavior
Tumialan et al. [50]	CFRP	100%	55%	55%	Premature shear failure in masonry
Verderame et al. [51]	CFRP/GFRP	10.5 kN	6.3–7.0 kN	60–67%	Early interfacial delamination limits strength
D'Antino et al. [52]	FRCM	100%	90–95%	90–95%	High agreement between model and test

Papanicolaou et al. [53]	TRM	100%	85–100%	85–100%	Progressive failure, stable structural behavior
Ricci et al. [54]	FRCM	11.5 kN	10.0–10.2 kN	87–89%	Matches well with virtual work prediction

Given the consistent gap observed between theoretical predictions and experimental outcomes, particularly for externally bonded CFRP and GFRP systems, it is reasonable to introduce an empirical reduction factor when estimating the design moment capacity. Experimental studies have demonstrated that actual strength typically reaches only 40% to 60% of the theoretical values [49][50][51]. Accordingly, a conservative design approach may incorporate a global reduction factor ranging from 0.4 to 0.6, applied directly to the theoretical design moment. This adjustment accounts for premature debonding, brittle failure modes, and construction-related uncertainties. While such an approach is not yet universally adopted in existing design codes, it is supported by experimental evidence and improves the reliability of FRP retrofitting in real-world applications [51].

To better reflect this behavior in the analytical model, the MATLAB code was modified to incorporate this reduction factor when calculating the design moment. As shown in Figure 5.2-4, the resulting theoretical capacity, adjusted using a reduction factor of 0.45, is approximately 20.9 kN. This value closely matches the experimental peak load of 19.1 kN observed in the OOP_2E_FRP test specimen [46], indicating that the modified model provides a more realistic prediction aligned with experimental behavior.

```
clc; clear; close all;

%% ========================================================================
%  PARAMETERS: Geometry, Material Properties, and Safety Factors
% ========================================================================
% Geometry
W = 2.35;            % Wall width [m]
H = 1.83;            % Wall height [m]
t = 0.08;            % Wall thickness [m]
gamma = 0.336;       % Load eccentricity ratio (e/H)

% Masonry Properties
fm = 1.81e6;         % Masonry compressive strength [Pa]
```

ommand Window

```
--- Effective Design Strain Check ---
epsilon_fd (FRP rupture)    = 0.024615
epsilon_fdd (Debonding)     = 0.001612
epsilon_fe  (Controlling)   = 0.001612

=== DESIGN RESULTS ===
Unstrengthened Lateral Force             : 10.84 kN
Unstrengthened Moment                    : 0.71 kN·m

--- Strengthened Design (Controlled by epsilon_fe) ---
Maximum Strengthening Moment Mn (reduced): 1.37 kN·m
Reversed Lateral Force Fe (reduced)      : 20.94 kN
Controlling Failure Mode                 : FRP Rupture or Debonding
```

Figure 5.2-4 Strengthened design results after applying reduction factor (0.45 × Mn) derived from experimental efficiency observations.

5.2.2. FRCM-Strengthened Wall under Seismic Loading

To further validate the proposed theoretical model, three verification cases were analyzed using both MATLAB and Excel implementations. These include one unstrengthened masonry wall specimen (NR) and two strengthened configurations (G_120_R_1L and G_220_R_1L) using different types of FRCM systems depicted in Table 5-8and Table 5-9.

Table 5-8 Wall geometry and material properties for validation cases.

Loading Type	Width (m)	Height (m)	Thickness (m)	f_m (MPa)	E_m (GPa)	Axial Load (KN)
Seismic	1.08	1.2	0.2	3.3	0.5	50

Table 5-9 Properties of FRCM

Properties of FRCM	G_120_R_1L	G_220_R_1L
Thickness (mm)	0.024	0.036
Number of layers	1	1

Mortar thickness (mm)	15	15
Elastic modulus (N/mm^2)	72,000	67,000
Ultimate tensile strain (%)	1.8	1.68

In the first case, the unstrengthened wall (NR) was simulated using the virtual work approach. The resulting force-displacement curve did not align well with the experimental trend particularly, the model significantly overestimated the peak out-of-plane capacity, and the initial stiffness also deviated from the measured behavior. This discrepancy is attributed to the insufficient slenderness of the wall specimen, whose height-to-thickness (h/t) ratio falls below typical design recommendations. When the geometry does not allow for proper arching action to develop, the classical virtual work model tends to overpredict capacity, as depicted in Figure 5.2-5

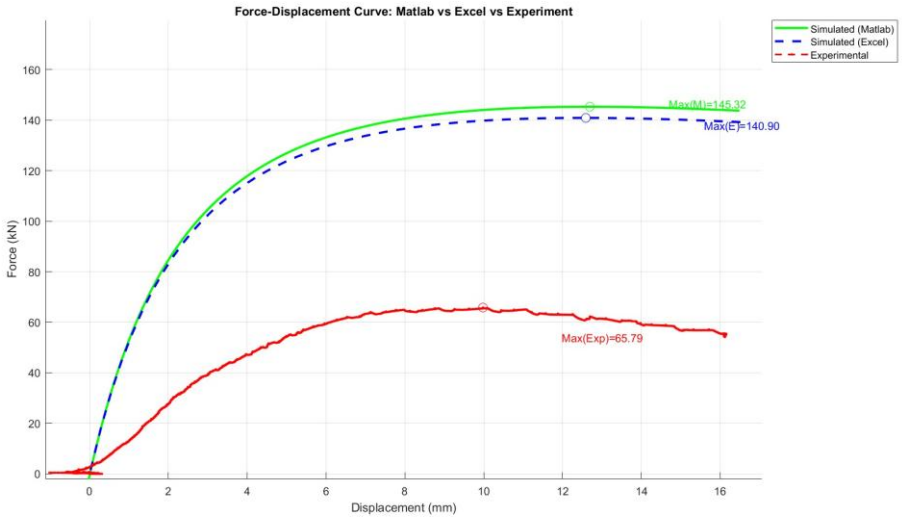

Figure 5.2-5 Force–displacement curve under seismic loading showing comparison between MATLAB simulation, Excel analysis, and experimental results.

However, by employing the CNR-DT 215/2018 design formulation for unstrengthened walls using Equation 3.2.2-9 and back-calculating the corresponding lateral force using the virtual work using Equation 3.1.1-8, the estimated out-of-plane force closely matches the experimental value, as shown in Table 5-10. This result demonstrates that even if the wall geometry does not meet standard h/t criteria, the virtual work principle remains applicable for reverse-engineering critical lateral actions when paired with reliable moment estimations.

Table 5-10 Comparison of moment capacity and out-of-plane strength of the unstrengthened wall obtained from different analytical and experimental methods.

	NR_Virtual	NR_CNR	NR_Experimental
Mn (KNm)	8.48	4.3	
F_{max} (KN)	140.91	71.5	65.79

For the second and third cases, the FRCM-retrofitted specimens G_120_R_1L and G_220_R_1L were analyzed by following the design procedure outlined in the CNR-DT 215/2018 guideline. The flexural capacity of each specimen was first computed using this procedure, where the effective strain of the FRCM system is conservatively defined as the minimum between the rupture strain and the end debonding strain, ensuring a safe-side estimation of the flexural moment.

As described in Section 3.2.2, the MATLAB-based implementation follows the same methodology by computing both potential failure design moments—one corresponding to masonry crushing and the other to FRCM rupture or debonding—and selecting the smaller value as the governing capacity. The moment capacities of both unstrengthened and strengthened masonry walls are determined within the same computational framework to ensure consistency. By applying the virtual work principle in reverse, as described in Equation 3.1.1-8, the corresponding maximum lateral force can be accurately estimated.

After evaluating the out-of-plane strength of the unstrengthened masonry wall, the same procedure is applied to the strengthened configurations. By substituting the calculated moment capacities into the virtual work formulation, the maximum lateral forces for each case are back-calculated. The results are summarized in Table 5-11, while Figure 5.2-6 and Figure 5.2-8 illustrate the corresponding maximum lateral forces computed in MATLAB using the design moments derived from the CNR-DT 215/2018 procedure.

The laboratory test setup used for experimental validation is shown in Figure 5.2-7 and Figure 5.2-9.

This approach enables a rapid and effective assessment of the strengthening strategy, allowing engineers to verify whether the retrofitting design provides sufficient improvement under expected loading conditions. By consistently adopting the conservative principle of using the lower value between rupture and debonding strain, the design ensures that the critical failure state is safely addressed.

Although a single design moment is adopted for safety considerations, it is important to highlight that, according to previous experimental studies [53][54], the actual failure mode

observed in FRCM-strengthened walls, whether governed by textile rupture or by debonding, may result in an experimental lateral capacity that lies between the values predicted by the two theoretical limit states. These potential discrepancies should be carefully considered when interpreting numerical predictions in comparison with experimental outcomes.

Table 5-11 Comparison of Predicted and Experimental Out-of-Plane Strength for FRCM-Strengthened Walls.

	G_120_R_1L	**G_220_R_1L**
F_{max} (KN), from ε_{fd}	100.11	109.04
Experimental F_{max} (KN)	93.22	111.42

```
36    fctm = 1.5e6;                    % [Pa] Masonry tensile strength
37    FC = 1.2;                          % [-] Knowledge level factor
38    su = 0.0004;                     % [m] Effective slip
39
40    % FRCM Properties
41    % Debonding Control Parameters
42    Ef = 72e9;                           % [Pa] elastic modulus of the dry fabric
43    epsilon_uf = 0.018;                  % [-] characteristic value of the ultimate strain of the dry fabric
44    sigma_uf = Ef * epsilon_uf;          % [N/m] characteristic value of the ultimate stress of the dry fabric
45
46    epsilon_u=0.0144 ;                    %average value of the ultimate strain of the FRCM strengthening
47    sigma_u = Ef * epsilon_u;            % [Pa] characteristic value of the ultimate stress of the FRCM strengthe
48
49    epsilon_lim_conv = 0.0108;           % [-] strain corresponding to on the tensile curve of the dry fabric)
50    sigma_lim_conv = Ef * epsilon_lim_conv;%characteristic value of the debonding capacity
51
52
```

```
mmand Window

================== FINAL RESULTS ==================
▶ M0d (Unstrengthened Moment)            : 4.30 kN·m
▶ MRd (Design Moment)                    : 6.03 kN·m

================== LATERAL FORCE ESTIMATION ==================
▶ Reversed Lateral Force (Fe@M0d)        : 71.53 kN
▶ Reversed Lateral Force (Fe@MRd)        : 100.11 kN

================== SUMMARY ==================
▶ Failure Mode                           : FRCM Rupture or Debonding
```

Figure 5.2-6 MATLAB output for G_120_R_1L specimen: design moment, reversed lateral force, and failure mode estimation based on CNR-DT 215/2018.

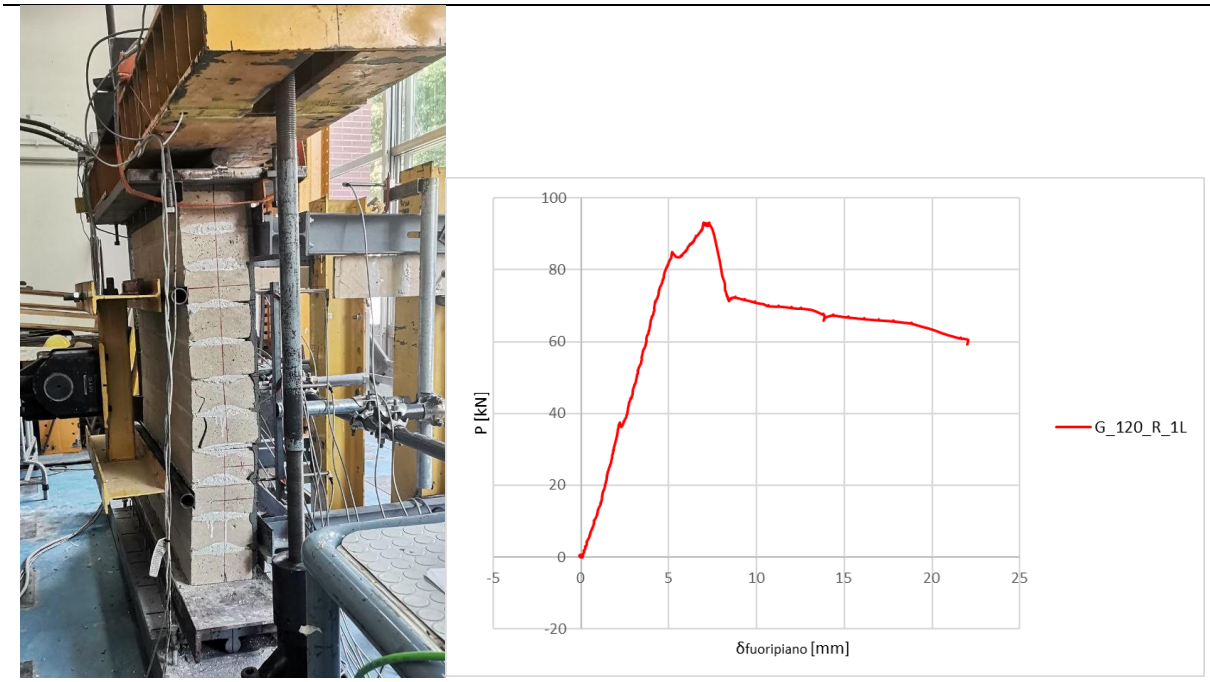

(a) (b)

Figure 5.2-7 (a) Experimental setup and (b) out-of-plane load–displacement response of specimen G_120_R_1L under seismic loading.

```
kgk = 0.15;                          % [-] Bond coefficient
fctm = 1.5e6;                        % [Pa] Masonry tensile strength
FC = 1.2;                              % [-] Knowledge level factor
su = 0.0004;                         % [m] Effective slip

% FRCM Properties
% Debonding Control Parameters
Ef = 67e9;                              % [Pa] elastic modulus of the dry fabric
epsilon_uf = 0.018;                     % [-] characteristic value of the ultimate strain of the dry fabric
sigma_uf = Ef * epsilon_uf;             % [N/m] characteristic value of the ultimate stress of the dry fabric

epsilon_u=0.0144 ;                       %average value of the ultimate strain of the FRCM strengthening
sigma_u = Ef * epsilon_u;               % [Pa] characteristic value of the ultimate stress of the FRCM strengthe

epsilon_lim_conv = 0.010752;              % [-] strain corresponding to on the tensile curve of the dry fabric)
sigma_lim_conv = Ef * epsilon_lim_conv;%characteristic value of the debonding capacity
```

```
ommand Window

================== FINAL RESULTS ==================
▶ M0d (Unstrengthened Moment)            : 4.30 kN·m
▶ MRd (Design Moment)                    : 6.56 kN·m

================== LATERAL FORCE ESTIMATION ==================
▶ Reversed Lateral Force (Fe@M0d)        : 71.53 kN
▶ Reversed Lateral Force (Fe@MRd)        : 109.04 kN

================== SUMMARY ==================
▶ Failure Mode                           : Masonry Crushing
```

Figure 5.2-8 MATLAB output for G_220_R_1L specimen: design moment, reversed lateral force, and failure mode estimation based on CNR-DT 215/2018.

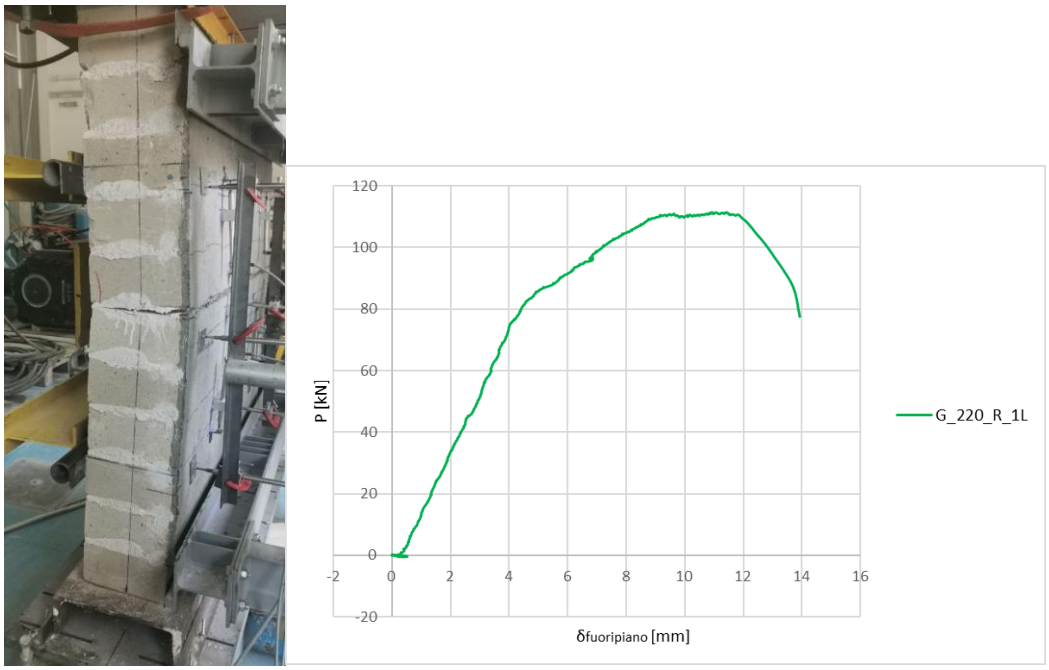

(a) (b)

Figure 5.2-9 (a) Experimental setup and (b) out-of-plane load–displacement response of specimen G_220_R_1L under seismic loading.

5.2.3. FRCM-Strengthened Wall under Tsunami Loading

To validate the tsunami load simulation for FRCM-strengthened masonry walls, the configuration labeled G_120_R_1L was selected, with wall properties defined in Table 5-3 and strengthening details provided in Table 5-9. The experimental setup used for validation is shown in Figure 5.1-6.

This configuration was analyzed using the MATLAB framework based on the virtual work principle. The computed lateral force and moment capacity were compared with the corresponding experimental results.

The experimental response is presented in Figure 5.2-11, while the theoretical prediction from the simulation is shown in Figure 5.2-10. Under tsunami loading conditions, the experimental test recorded a peak out-of-plane lateral force of 108.00 kN, and the simulation predicted a corresponding value of 103.20 kN. The difference between the two results is approximately 4.4 percent, indicating that the proposed model accurately captures the structural behavior of masonry walls strengthened with FRCM under tsunami loading.

```
clc; clear; close all;

%% ================================================================
%  INPUT PARAMETERS — STRUCTURAL GEOMETRY, MATERIALS, LOADS
% ================================================================

% Geometry
W = 4.2;            % [m] Wall width
H = 2.3;            % [m] Wall height
t = 0.12;           % [m] Wall thickness
gamma = 0.24;       % [-] Load eccentricity ratio (virtual work)
```

```
ommand Window
=== MAXIMUM VALUES (UNSTRENGTHENED) ===
Max Equivalent Lateral Force Fe = 51.53 kN
Corresponding R1 = 48.11 kN, h1 = 0.46 m
Corresponding R2 = 3.42 kN, h2 = 1.03 m
Maximum Moment M = 1.54 kN·m
Tsunami Height Hw = 1.46 m

=== REVERSE ANALYSIS: Masonry Crushing ===
Target MRd = 3.53 kN·m
Approximated M = 3.53 kN·m (error = 0.03%)
Fe = 103.20 kN
R1 = 79.54 kN, h1 = 0.51 m
R2 = 23.66 kN, h2 = 0.80 m
Tsunami Height Hw = 2.11 m
```

Figure 5.2-10 MATLAB output for G_120_R_1L specimen: design moment, reversed lateral force, and critical tsunami height based on CNR-DT 215/2018.

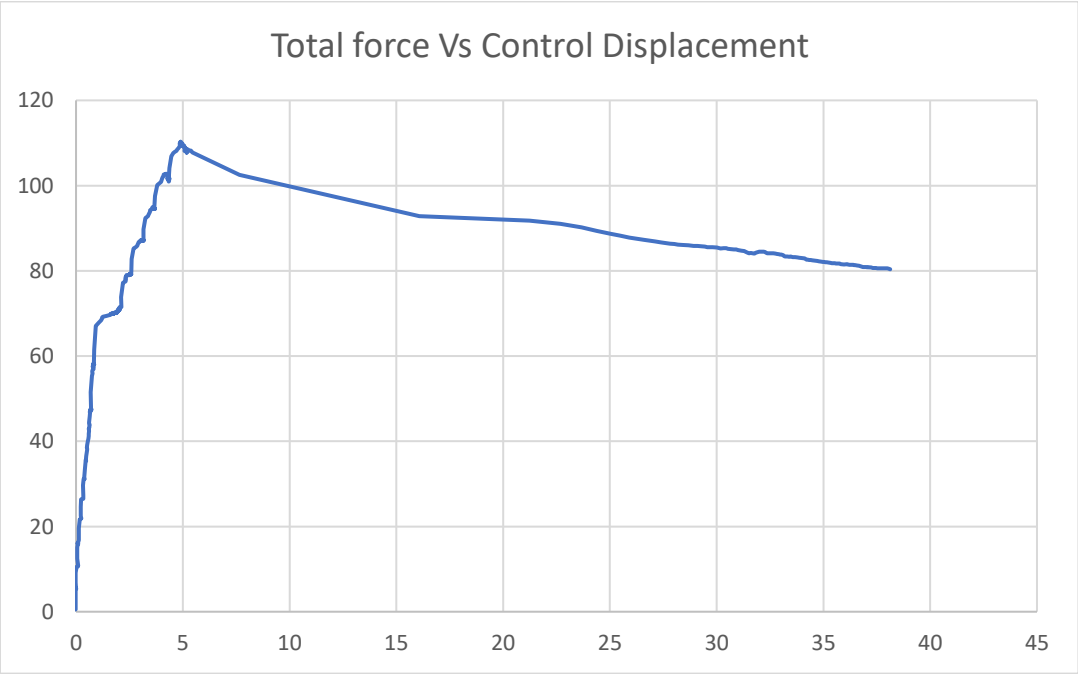

Figure 5.2-11 Out-of-plane load–displacement response of specimen G_120_R_1L under tsunami loading.

5.3. Influence of Wall Slenderness Ratio (h/t) on the Accuracy of the Virtual Work Method

The slenderness ratio (height-to-thickness, h/t) of masonry walls plays a critical role in determining the effectiveness of arching action and, consequently, the applicability of the virtual work method for estimating out-of-plane (OOP) capacity.

According to widely accepted design guidelines, conservative limits are recommended to ensure proper arching behavior. The ASCE/SEI 41-13 specifies a minimum slenderness ratio of $h/t \geq 25$, which is increased to 35 in the updated ASCE/SEI 41-17. Eurocode 8, on the other hand, typically adopts $h/t \geq 15$ as a conservative lower bound.

However, some experimental and numerical studies indicate that partial arching action may begin to develop under certain conditions, even when $h/t \geq 10$, depending on boundary conditions and stiffness characteristics [57][58].

Despite this, most literature agrees that when $h/t < 15$, the development of out-of-plane arching behavior is limited or unstable, with unreliable force transmission mechanisms [57] [58] [59]. Conversely, when $h/t \geq 20–25$, the arching mechanism becomes more stable and significantly enhances the wall's out-of-plane resistance [37].

This relationship is clearly reflected in the two unstrengthened wall specimens analyzed in this study. Specimen 4.1.1, discussed in Section 4.1.1, had an h/t ratio of 9.6—close to the threshold where arching begins to occur [57]. These observations are also consistent with several studies suggesting that arching action may begin to develop when the slenderness ratio exceeds 10, even if it does not reach the commonly accepted code threshold of 15. Under certain boundary conditions, partial arching behavior has been observed experimentally at $h/t \geq 10$, enabling limited out-of-plane resistance enhancement [57][58][59].

Accordingly, the virtual work method produced a force-displacement response that roughly aligns with the experimental data.

In contrast, Specimen 4.2.2, presented in this section, has a significantly lower h/t ratio of 6, which is well below standard code limits. As a result, the virtual work formulation failed to capture realistic behavior and significantly overestimated both initial stiffness and ultimate capacity due to the lack of an effective arching mechanism, as depicted in Table 5-12.

These findings underscore the importance of evaluating wall slenderness when applying the virtual work method, particularly for configurations with non-standard geometries or boundary conditions.

Table 5-12 Comparison of Wall Geometry and Slenderness.

	Height (m)	Thickness (m)	slenderness ratio (H/t)
Table 5-1	1.16	0.12	9.6
Table 5-2	1.83	0.08	22.87
Table 5-3	2.3	0.12	19.16
Table 5-8	1.2	0.2	6

5.4. Optimization of Slenderness Verification and Limitations of the Virtual Work Approach at Low h/t

To unify the findings from Sections 5.1 and 5.2, this section presents an optimized modeling workflow that incorporates slenderness verification at the initial stage of the virtual work implementation in MATLAB. Specifically, the slenderness ratio h/t is automatically checked to determine whether it satisfies the Eurocode 8 lower-bound recommendation of $^{h}/_{t} \geq 15$ If the wall geometry fails to meet this criterion, a warning message is displayed:

"Warning: h/t ratio is below the recommended threshold. The results may not reflect realistic behavior.", as depicted in Figure 5.4-1.

Despite this limitation, the analysis proceeds by applying the virtual work principles to compute the complete force-displacement response. This is particularly useful for conceptual comparison and for assessing the potential enhancement from retrofitting systems.

As depicted in Figure 5.4-1, when the wall has a low slenderness ratio (e.g., $^{h}/_{t} \geq 15$), the virtual work-based response curve tends to significantly overestimate both the initial stiffness and the peak out-of-plane capacity, deviating markedly from experimental trends. This behavior confirms that the virtual work method becomes unreliable for force prediction under insufficient geometric conditions where arching action cannot fully develop.

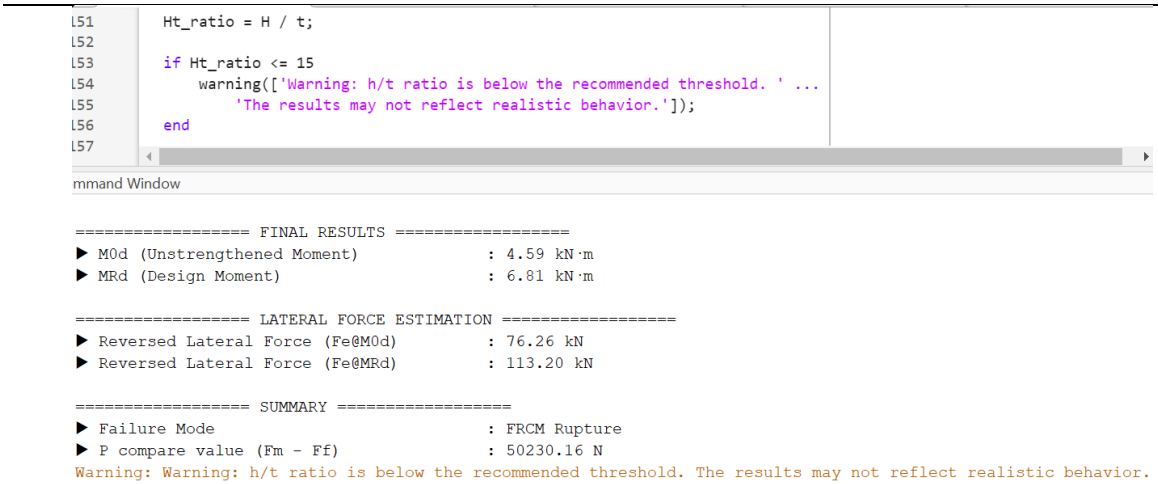

Figure 5.4-1 Warning message displayed when the height-to-thickness ratio (h/t) is below the recommended threshold of 15. Such conditions may lead to unrealistic behavior in the structural response analysis.

However, it is worth noting that the computed displacement at peak shows reasonable agreement with experimental measurements. Although the predicted lateral force may not be a reliable design value, the virtual work method can still offer a valuable estimate of the maximum displacement that an unstrengthened wall might undergo. This insight can assist engineers in evaluating deformation compatibility and understanding the behavior of the wall before retrofitting.

In contrast, once the design moment is obtained through the CNR-DT 215/2018 and CNR-DT 200/2025 procedure—either from rupture strain or end debonding strain—the corresponding maximum lateral force can still be reliably computed through Equation 3-8. This confirms the validity of the hybrid approach for strengthened walls, regardless of geometric limitations.

5.5.Monte Carlo Simulation and Probabilistic Evaluation

To evaluate the probabilistic structural performance and variability of FRP/FRCM strengthened masonry walls under tsunami and seismic loads, a Monte Carlo simulation was conducted. This method allows for a large number of randomized input samples to be evaluated, capturing uncertainties in geometry, material properties, and reinforcement configurations. Unlike the deterministic analyses presented in Sections 5.1 and 5.2, which focused on single-case validation, this stochastic approach helps quantify the range of possible outcomes and failure modes across a broader design space.

The input parameters for the simulation, along with their respective probability distributions and ranges, are summarized in Table 5.13. A total of 50,000 random samples were generated using predefined ranges for each variable. These samples were then fed into the MATLAB framework introduced earlier to automatically compute the design moment, failure mode, and corresponding tsunami flood force for each configuration.

The results of this probabilistic analysis, including fragility distribution plots and comparative performance metrics for each strengthening technique, are discussed in detail in Chapter 6.

Table 5-13 Monte Carlo Input Parameters and Statistical Distribution.

Category	Parameter	Description	Distribution	Value Range / Mean (± COV)
Masonry	f_m	Compressive strength of masonry	Lognormal	1.5 MPa (±14%)
	E_m	Elastic modulus of masonry	Lognormal	1.8 GPa (±14%)
	t	Wall thickness	Random	0.12 – 0.24 m
	H	Wall height	Random	2.5 – 3.2 m
	W	Wall width	Random	4.0 – 6.0 m
Load	γ	Load eccentricity ratio	Random	0.15 – 0.30
	P	Axial load	Constant	0
	ρ_sea	Density of seawater	Constant	1.2 ton/m³
	vt	Tsunami velocity	Random	2 – 6 m/s
	ρ_flood	Density of floodwater	Constant	1.0 ton/m³
	v_flood	Flood velocity	Constant	0
	ppf	Pyroclastic flow pressure	Random	10 – 40 kPa
CFRP	t_f	Thickness (dry)	Constant	0.337 mm
	w_s	Strip width	Random	0.05 – 0.20 m
	s	Strip spacing	Random	0.10 – 0.25 m
	f_{fc}	Tensile strength	Lognormal	4000 MPa (±20%)
	E_{fc}	Elastic modulus	Lognormal	250 GPa (±20%)
	n	Number of layers	Random	1 or 2
GFRP	t_f	Thickness (dry)	Constant	0.342 mm
	w_s	Strip width	Random	0.05 – 0.20 m
	s	Strip spacing	Random	0.10 – 0.25 m
	f_{fg}	Tensile strength	Lognormal	2000 MPa (±20%)
	E_{fg}	Elastic modulus	Lognormal	70 GPa (±20%)
	n	Number of layers	Random	1 or 2
FRCM	t_m	Mortar thickness	Random	0.15 – 0.30 m
	t_{f_grid}	Grid thickness	Constant	0.036 mm
	f_f	Grid tensile strength	Lognormal	1200 MPa (±20%)
	E_{fg}	Grid elastic modulus	Lognormal	70 GPa (±20%)
	n	Number of layers	Random	1 or 2

6. PROBABILISTIC PERFORMANCE ASSESSMENT UNDER SEISMIC AND TSUNAMI LOADING

6.1. Introduction

This chapter presents the probabilistic results derived from Monte Carlo simulations performed on both unstrengthened and retrofitted masonry wall systems. The aim is to assess the variability and reliability of design moment capacities under seismic loading, and to extend the same framework to tsunami-induced scenarios later.

Unlike deterministic analysis, which a single output for a given set of parameters, the Monte Carlo approach incorporates statistical variation in material properties, geometric dimensions, and reinforcement characteristics. This allows for a more comprehensive understanding of structural performance under uncertainty, providing insight into the likely range of design strengths and the distribution of failure modes.

Through this analysis, the study evaluates the consistency of the numerical framework and quantifies the difference in behavior between strengthening systems such as CFRP, GFRP, and FRCM. The chapter begins by analyzing the statistical distribution of the design moment Mn for seismic conditions and subsequently interprets the equivalent hydrodynamic responses under tsunami loading.

6.2. Statistical Distribution under Seismic Loading

To evaluate both the capacity and statistical variability of URM walls under seismic action, two key structural indicators were assessed: the flexural design moment capacity Mn, calculated based on strength design principles, and the equivalent out-of-plane force, derived using the virtual work method to represent the seismic-induced lateral force demand. These parameters collectively represent the supply-demand balance in out-of-plane wall behavior.

Monte Carlo simulations were conducted using 50,000 samples per wall configuration (unstrengthened, CFRP, GFRP, and FRCM retrofitted), based on probabilistic distributions of key inputs such as wall geometry, masonry strength, and reinforcement properties, as defined in Chapter 5. This approach allows for quantifying not only the expected performance but also the level of uncertainty associated with each strengthening strategy.

Figure 6.2-1 and Figure 6.2-2 present the fragility function of Mn and OOP force, respectively. The results reveal that unstrengthened walls show the lowest moment capacity with minimal variation an indication of inherently poor seismic performance but statistically consistent behavior. Once retrofitted, the walls show substantial improvements in both indicators, albeit with differences in statistical dispersion and central tendency.

CFRP-retrofitted walls demonstrate the highest maximum values in both Mn and OOP force, implying a strong capacity enhancement potential. However, their CDFs are also the most dispersed, indicating high sensitivity to input variability, especially related to fiber strain limits, debonding behavior, and installation quality. This observation highlights the importance of more consistent median values. FRCM, in particular, exhibits lower variability across the samples, which may be attributed to its composite behavior and mechanical anchorage through mesh matrix interaction, making it less sensitive to bonding conditions than CFRP. GFRP also performs reasonably well but with slightly higher variability, likely due to lower modulus and strength compared to CFRP.

From a design view, these differences have practical implications. While CFRP may offer the highest theoretical resistance, it also requires stricter design checks and quality control. In contrast, FRCM may provide more reliable performance in real-world conditions with less sensitivity to parameter fluctuation. strict material control and workmanship in CFRP applications.

Among the retrofitted walls, FRCM exhibits the most compact and stable statistical distribution, whereas GFRP and CFRP show similarly high variability. These trade-offs between strength and consistency must be carefully considered when selecting a retrofitting system for seismic or tsunami resilience.

A summary of statistical indicators—including mean, standard deviation, coefficient of variation (COV), and key percentiles (P5, P50, P95)—is provided in Table 6-1for Mn and Table 6-2 for OOP force. These allow for quantitative comparisons across the strengthening schemes in terms of both central tendency and reliability.

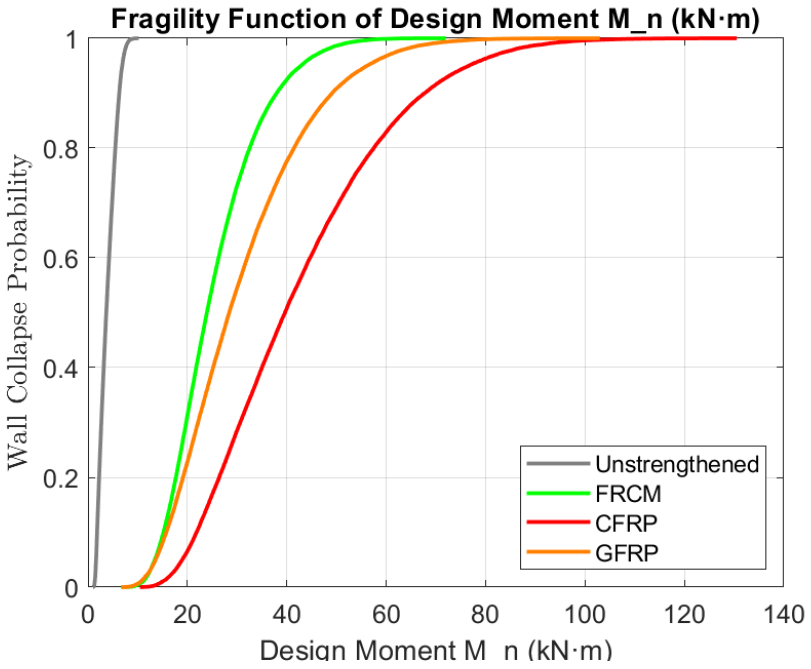

Figure 6.2-1 Fragility functions of design moment Mn for unstrengthened and retrofitted masonry walls under seismic loading.

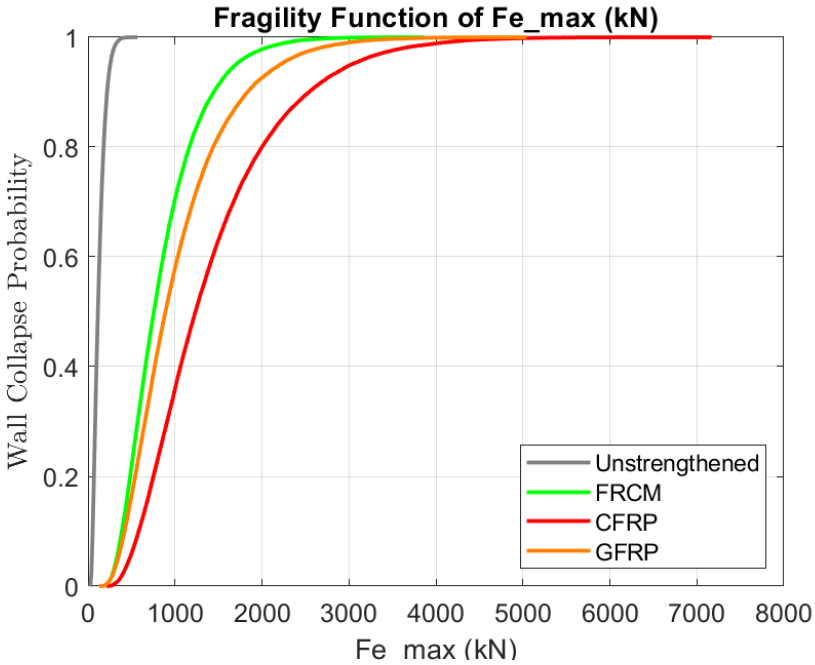

Figure 6.2-2 Fragility functions of equivalent out-of-plane force under seismic loading for different wall types.

Table 6-1 Statistical summary of design moment Mn (KN·m).

Wall Type	Mean	Std Dev	COV	P5	P95
Unstrengthened	3.90	1.68	0.43	1.63	6.89
FRCM	25.44	9.01	0.35	13.44	42.84
GFRP	30.79	13.24	0.43	13.61	56.16
CFRP	42.58	17.94	0.42	18.95	76.62

Table 6-2 Statistical summary of equivalent Out-of-Plane force (KN).

Wall Type	Mean	Std Dev	COV	P5	P95
Unstrengthened	127.18	66.72	0.52	45.11	255.22
FRCM	851.44	437.94	0.51	328.84	1697.22
GFRP	1030.16	592.08	0.57	344.25	2207.86
CFRP	1425.10	809.00	0.57	477.90	3020.98

6.3. Statistical Distribution under Tsunami and Flood Loading

In addition to seismic loading, the out-of-plane performance of masonry walls was also evaluated under tsunami-induced hydrodynamic loading. The tsunami and flood scenario introduces a progressive fluid pressure profile, where the inundation depth Hw governs the magnitude and distribution of lateral forces. To capture the resulting structural response, three key variables were analyzed: the tsunami height Hw, the total out-of-plane force Fe, and design moment Mn.

The fragility function was generated using 50,000 Monte Carlo samples for each wall type. These plots provide a probabilistic view of how different retrofitting systems respond to tsunami forces. As depicted in Figure 6.3-1 CDF of tsunami height Hw illustrates that strengthened walls are associated with higher inundation depths compared to unstrengthened walls. This is consistent with their capacity to withstand greater fluid forces. For example, the mean tsunami height for CFRP-retrofitted walls is 8.7 m, while that of unstrengthened walls is only 2.0 m, indicating a much lower capacity to resist tsunami loading.The corresponding statistical summary is provided in Table 6-3.

The fragility functionof out-of-plane force Fe is presented in Figure 6.3-2 in the cases, CFRP-retrofitted walls demonstrate the highest mean values among all wall types, with an average out-of-plane force of 1180.3 kN and a base reaction force of 641.5 kN, as reported in Table 6-4. The coefficients of variation for CFRP is 0.46 for Fe, respectively, which are comparable to those of FRCM and GFRP systems. This suggests that while CFRP provides the highest capacity, its relative variability remains moderate and not significantly greater than other systems.

A comprehensive summary of statistical indicators including the mean, standard deviation, coefficient of variation, and key percentiles P5, P50, and P95 is presented in Table 6-3 for tsunami inundation height Hw, Table 6-4 for total out-of-plane force Fe,and Table 6-5 for the design moment Mn. These statistical summaries enable clear and quantitative comparisons

among the different strengthening schemes, highlighting both their average performance and the variability associated with each system.

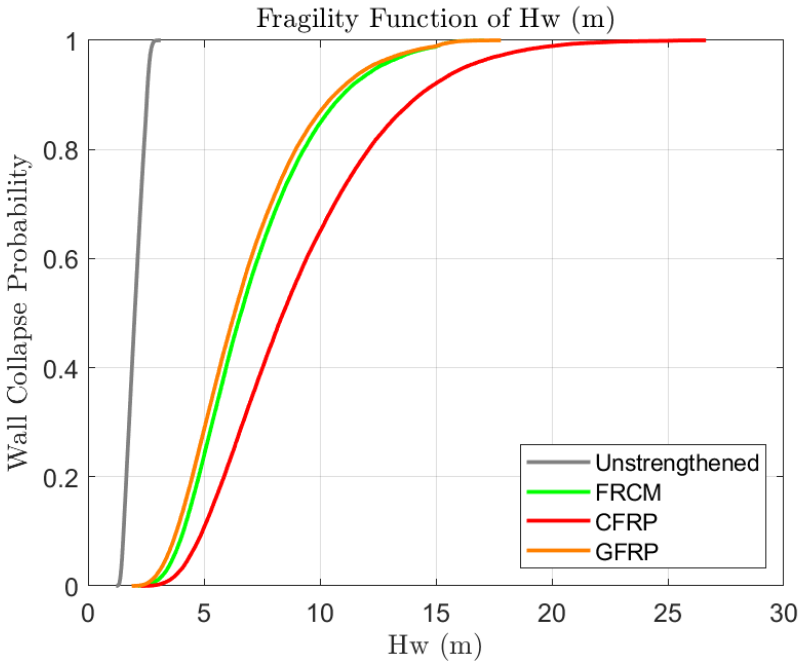

Figure 6.3-1 Fragility functions of Tsunami inundation height (m) for each wall type under tsunami-induced loading.

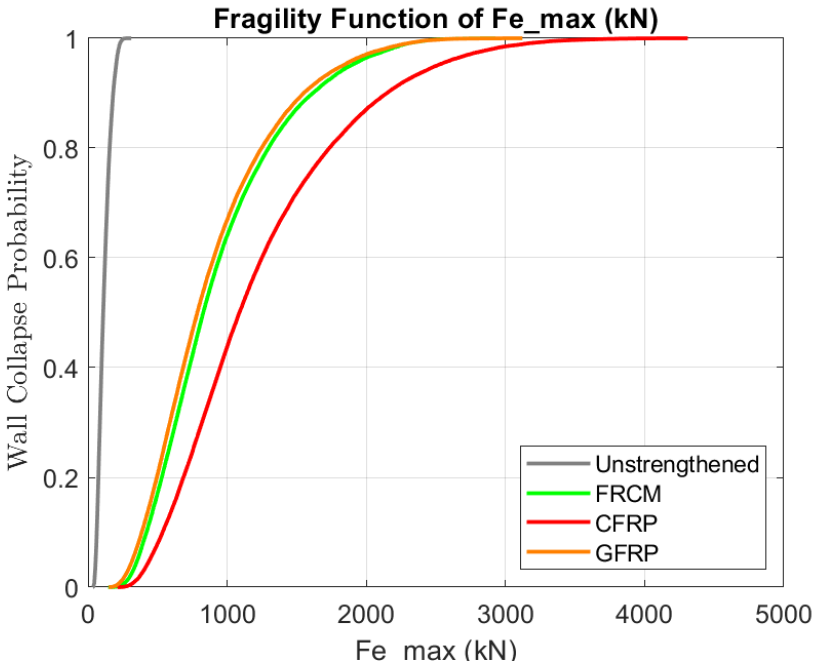

Figure 6.3-2 Fragility functions of equivalent out-of-plane Force Fe_{max} (KN) under tsunami-induced loading.

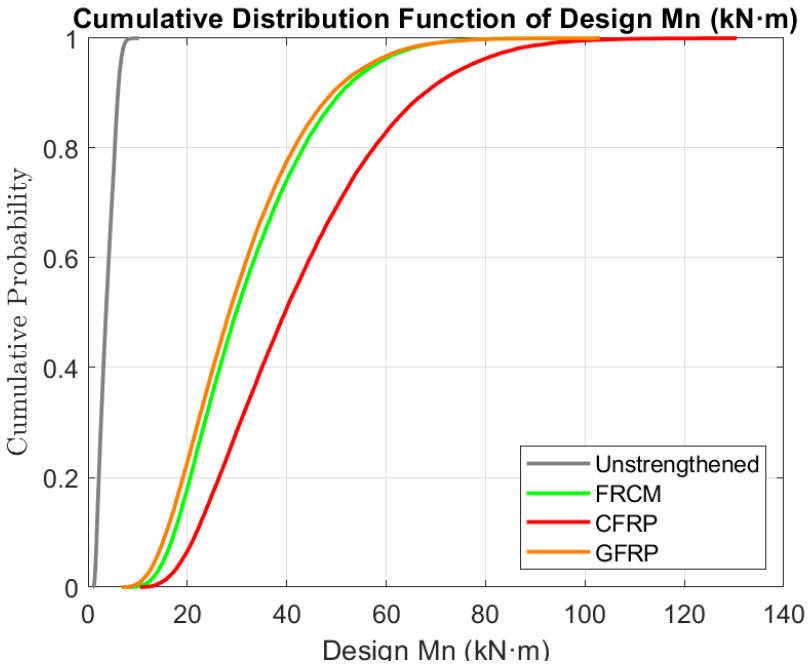

Figure 6.3-3 Fragility functions of design Moment Mn (KN·m) under tsunami-induced loading.

Table 6-3 Statistical summary of Tsunami height Hw (m).

Wall Type	Mean	Std Dev	COV	P5	P95
Unstrengthened	2.03	0.37	0.18	1.47	2.63
FRCM	7.09	2.60	0.37	3.65	12.47
GFRP	6.80	2.60	0.38	3.37	12.10
CFRP	8.78	3.04	0.35	4.33	13.73

Table 6-4 Statistical summary of Out-of-Plane force (KN).

Wall Type	Mean	Std Dev	COV	P5	P95
Unstrengthened	116.26	44.92	0.39	55.51	201.44
FRCM	926.23	451.56	0.49	355.88	1839.80
GFRP	883.71	448.39	0.51	320.26	1798.09
CFRP	1180.35	537.59	0.46	443.64	2160.37

Table 6-5 Statistical summary of design moment Mn (KN·m).

Wall Type	Mean	Std Dev	COV	P5	P95
Unstrengthened	3.80	1.61	0.42	1.57	6.53
FRCM	32.06	12.66	0.39	15.29	55.31
GFRP	30.57	12.74	0.42	13.62	54.25
CFRP	41.03	15.47	0.38	18.97	68.46

Compared to tsunami scenarios, the fragility behavior of unreinforced masonry walls under flood loading follows a similar trend in terms of collapse probability versus moment capacity and lateral force. However, for the same level of structural resistance such as design moment or equivalent out-of-plane force, flood-induced loads require slightly greater inundation depths

due to their purely hydrostatic nature and the linearly increasing pressure profile with depth. Despite this variation in water depth, the statistical patterns, including the effectiveness of each retrofit type, the variability in performance, and the overall reliability, remain consistent with those observed under tsunami-induced conditions. As shown in Figure 6.3.X, the fragility functions under flood loading for design moment, lateral force, and inundation depth display comparable curve shapes and separations among the different strengthening systems, confirming the robustness and consistency of the probabilistic trends across both hazard types.

A comprehensive summary of statistical indicators including the mean, standard deviation, coefficient of variation, and key percentiles P5, P50, and P95 is presented in Table 6-3 for tsunami inundation height Hw, Table 6-4 for total out-of-plane force Fe,and Table 6-5 for the design moment Mn. These statistical summaries enable clear and quantitative comparisons among the different strengthening schemes, highlighting both their average performance and the variability associated with each system.

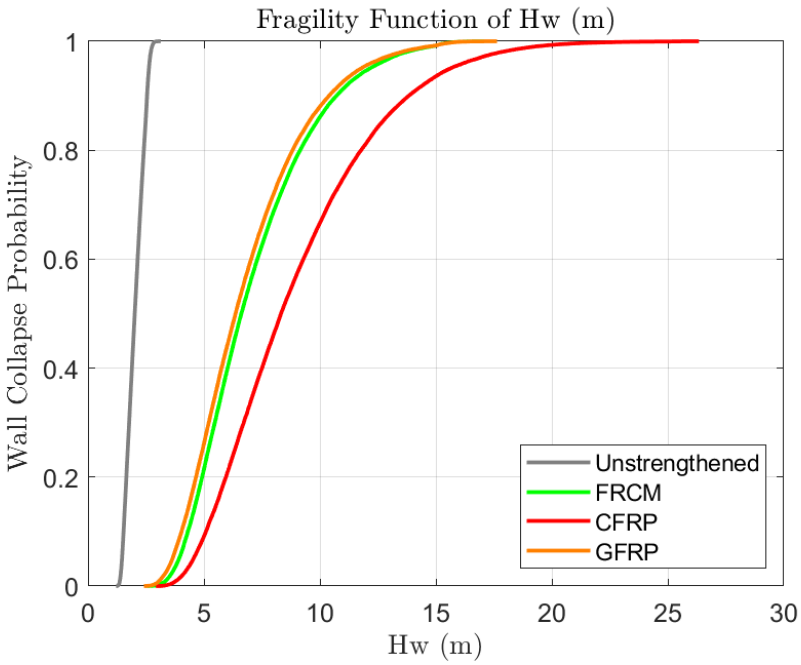

Figure 6.3-4 Fragility functions of Tsunami inundation height (m) for each wall type under flood-induced loading.

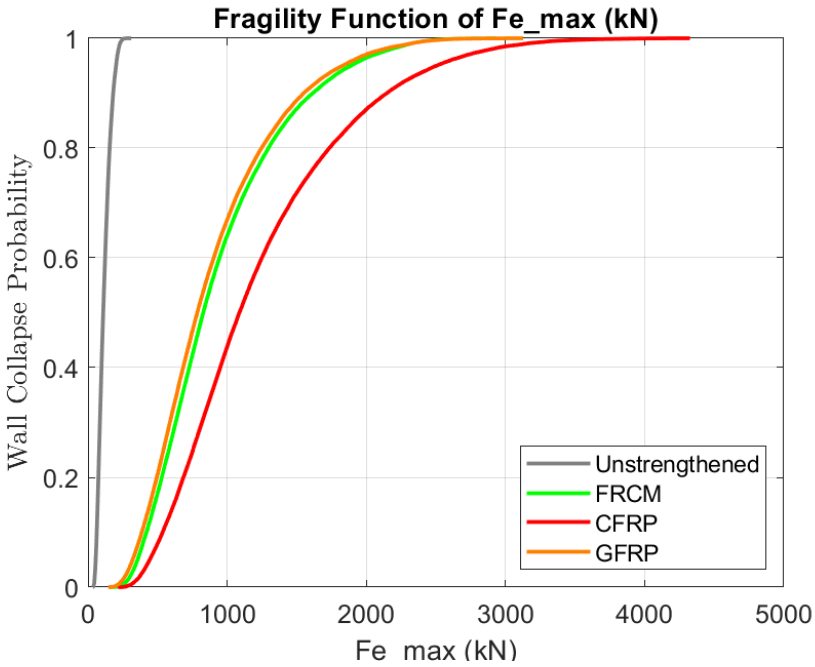

Figure 6.3-5 Fragility functions of equivalent out-of-plane Force Fe_{max} (KN) under flood-induced loading.

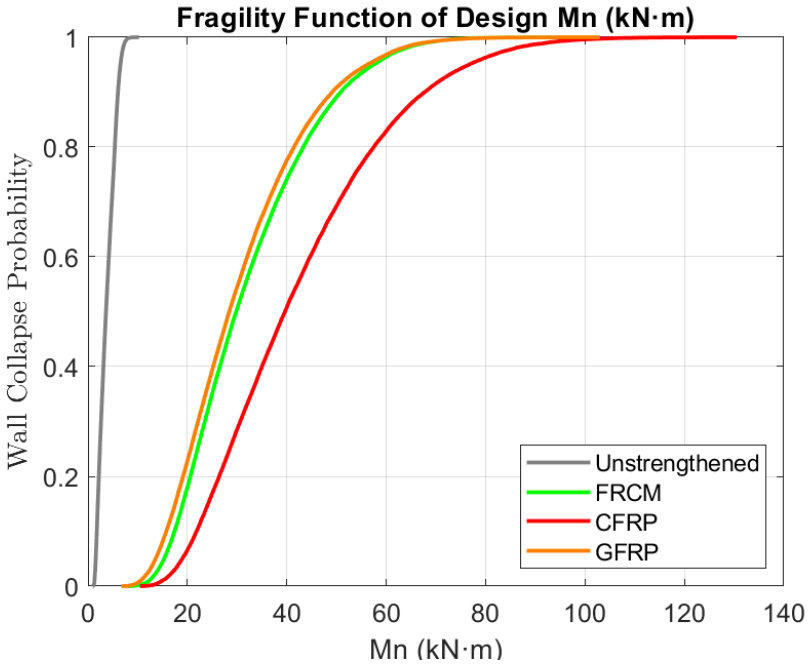

Figure 6.3-6 Fragility functions of design Moment Mn (KN·m) under flood-induced loading.

Table 6-6 Statistical summary of Tsunami height Hw (m).

Wall Type	Mean	Std Dev	COV	P5	P95
Unstrengthened	2.03	0.37	0.18	1.47	2.63
FRCM	7.13	2.54	0.36	3.92	12.15
GFRP	6.85	2.53	0.37	3.64	11.77
CFRP	8.99	3.48	0.39	4.55	15.62

Table 6-7 Statistical summary of Out-of-Plane force (KN).

Wall Type	Mean	Std Dev	COV	P5	P95
Unstrengthened	116.26	44.92	0.39	55.51	201.44
FRCM	933.60	469.59	0.50	356.53	1890.36
GFRP	890.28	465.22	0.52	320.50	1829.59
CFRP	1233.12	639.87	0.52	443.63	2504.10

Table 6-8 Statistical summary of design moment Mn (KN·m).

Wall Type	Mean	Std Dev	COV	P5	P95
Unstrengthened	3.80	1.61	0.42	1.57	6.53
FRCM	32.30	13.16	0.41	15.30	57.37
GFRP	30.79	13.24	0.43	13.61	56.16
CFRP	42.58	17.94	0.42	18.95	76.62

Figure 6.3.3 presents the fragility functions of Hw under both tsunami and flood-induced loading scenarios. The results show that although retrofitted walls exhibit similar collapse probabilities at equivalent moment capacities, the required water depths differ significantly between tsunami and flood conditions.

For the exact target moment,tsunami-induced loading typically results in lower Hw values compared to flood loading. This difference arises primarily from the nature of the applied loads. Flood-induced pressure is entirely hydrostatic, increasing linearly with depth as water gradually accumulates over time. In contrast, tsunami loading consists of both hydrostatic and hydrodynamic components. The hydrodynamic part is associated with the momentum of fast-moving water impacting the wall surface, resulting in higher forces over shorter durations. These forces tend to concentrate on the upper portion of the wall, resulting in higher overturning moments, even when the inundation depth is relatively shallow. However, when the inundation depth exceeds approximately 12–15 meters, a significant reversal in collapse probability is observed: the fragility curves under flood conditions surpass those of tsunami scenarios. This phenomenon is particularly evident for CFRP- and FRCM-strengthened walls and can be explained through the underlying mechanics of the applied loading models.

According to Eq. (1), flood loads are modeled as hydrostatic and linearly increasing with depth. The total force is given by equation 3.1.2-7, indicating a quadratic growth with water depth and a pressure distribution concentrated near the wall base. Combined with long-duration exposure, this creates increasingly severe loading at deeper inundation depths, leading to premature failure at the base or interfaces.

In contrast, tsunami-induced loads follow hydrodynamic models defined in equations 3.1.2-8 and 3.1.2-9, where the total force scales with the square or fourth power of the flow velocity. As described in equation 3.1.2-10, flow velocity is inversely proportional to the square root of

water depth Hw, implying that tsunami forces tend to saturate or grow more slowly with increasing depth due to energy dissipation and reduced velocity.

Therefore, while tsunami loads dominate at shallow depths due to the effects of dynamic pressure, flood-induced forces become more significant at greater inundation depths. This is primarily due to their quadratic dependence on water depth, extended duration of action, and pressure concentration closer to the wall base. These characteristics are especially critical under conservative design assumptions or for structural systems that are sensitive to stress accumulation near the base.

Additionally, this reversal is further supported by the fundamental difference in how the two hazards scale with depth. At low to moderate water levels, tsunami loading tends to be more destructive because it includes dynamic pressure effects driven by flow velocity and Froude number. However, as water depth increases, the flow velocity may decrease due to energy dissipation, and the Froude number may fall below critical thresholds. This reduction in flow momentum causes the tsunami-induced force to saturate or grow at a slower rate. On the other hand, flood loads are modeled as purely hydrostatic and scale with the square of the water depth, which results in a much faster increase in lateral force as the inundation depth rises. Consequently, under high water conditions, flood scenarios can produce greater damaging forces than tsunami scenarios, mainly when evaluated using conservative or simplified design assumptions.

Among the retrofitted systems, CFRP exhibits the best curve separation between tsunami and flood cases, indicating its sensitivity to pressure shape and location. FRCM shows more compact and stable statistical behavior, likely due to better mesh-matrix anchorage and distributed cracking. This comparison highlights that while tsunami loads are more hazardous at shallow depths, flood loads become dominant in deeper water; therefore, both scenarios must be considered in retrofit design.

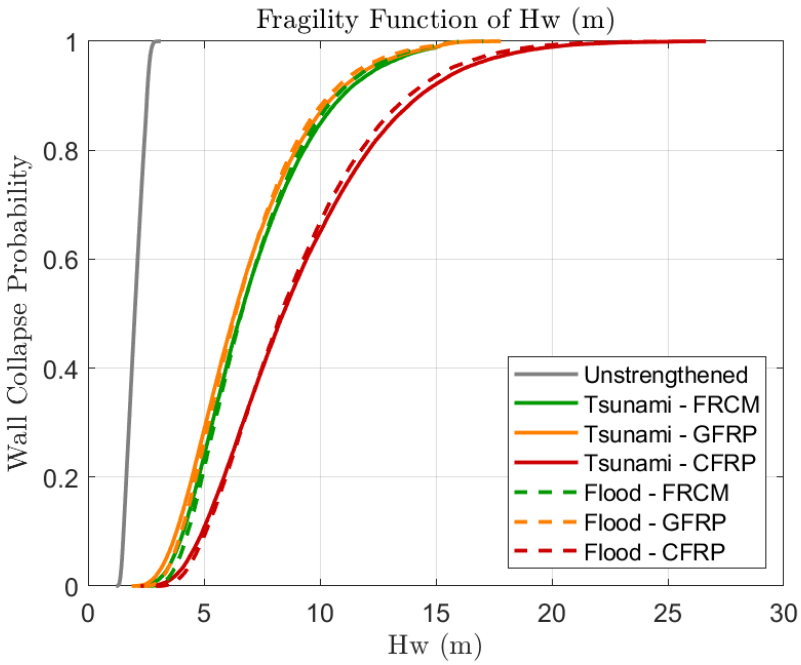

Figure 6.3-7 Comparison of fragility functions with respect to water depth (Hw) under tsunami and flood loading conditions.

6.4. Conclusions and Design Implications

The probabilistic analysis conducted in this chapter provides meaningful insights into the comparative reliability and variability of different strengthening systems for URM walls under seismic and tsunami/flood-induced loading. While CFRP systems demonstrate the highest average moment capacity and out-of-plane resistance, their relatively large coefficient of variation highlights the importance of quality control during installation and bond performance. On the other hand, FRCM systems exhibit lower variability and more consistent performance, making them preferable in cases where robustness and material compatibility are prioritized over peak strength.

The Monte Carlo simulations reveal that all strengthening systems significantly enhance the expected structural capacity compared to unstrengthened walls. However, the range of variability must be carefully considered in design. This study suggests that deterministic methods may overestimate the safety of FRP-retrofitted walls if bond degradation and variability are not explicitly accounted for. Including a probabilistic framework offers a more realistic assessment of structural performance and supports risk-informed design decisions, especially in tsunami-prone or high-seismicity regions.

THIS PAGE WAS INTENTIONALLY LEFT BLANK

7. CONCLUSION AND FUTURE WORK

7.1. Summary of Findings

This study proposed and validated a numerical modelling framework based on the principle of virtual work, enabling the analysis of out-of-plane behaviour of unreinforced masonry (URM) walls under both seismic and tsunami-induced loading. Through a combination of deterministic simulations and probabilistic Monte Carlo analysis, it was shown that composite strengthening systems such as FRP and FRCM can significantly enhance the structural performance of URM walls.

In deterministic scenarios, FRP-retrofitted walls achieved the highest theoretical moment capacities. However, the statistical analysis revealed that FRCM-retrofitted walls demonstrated more consistent performance with lower variation, particularly under tsunami loading. These findings confirm that while FRP offers higher peak strength, FRCM provides more reliable real-world effectiveness due to its better mechanical integration with masonry walls.

7.2.Contributions and Implications

This thesis makes several key contributions. First, it introduces a hybrid numerical methodology that merges code-based deterministic design procedures (based on CNR-DT 200 R2/2025 and CNR-DT 215/2018) with statistical reliability analysis via Monte Carlo simulations. This integration not only provides point estimates of strength but also offers a probabilistic envelope that captures uncertainty in geometry, materials, and installation variability.

Second, the study demonstrates that FRP design, if based solely on idealized strength values, may significantly overestimate wall safety due to premature debonding or brittle failure, as confirmed by multiple experimental studies. By comparing theoretical predictions with experimental data from the literature, it is evident that the actual out-of-plane strength of FRP-retrofitted walls often reaches only 40 to 60 percent of the calculated capacity. Therefore, this study recommends applying a reduction factor based on the experimental performance of similar wall configurations and materials to better align design values with realistic behavior.

Third, the framework supports multi-hazard retrofitting strategies by applying a unified energy-based approach (virtual work) to both seismic and tsunami scenarios. This establishes a

consistent basis for evaluating different strengthening systems under compound hazard conditions.

7.3. Limitations

Although the proposed model is practical and computationally efficient, it has several limitations. First, it adopts simplified boundary conditions, which may not fully represent complex support scenarios and can lead to deviations in the analysis results. Additionally, the model fails to capture nonlinear material behavior or crack propagation, thereby limiting its ability to simulate post-peak response and failure progression. Furthermore, when the wall slenderness ratio (height-to-thickness, h/t) is less than 15, the development of arching action becomes insufficient, reducing the accuracy of the virtual work method in representing out-of-plane behavior.

Additionally, while virtual work provides an elegant and efficient method for collapse load estimation, it does not include dynamic amplification, inertia effects, or time-dependent loading. These aspects are especially critical in tsunami scenarios where impact forces or debris loads may dominate.

Furthermore, the MATLAB code structure was modular but lacked full integration of probabilistic input variability in some deterministic modules. This aspect could be refined in future work to improve simulation cohesion.

7.4. Future Work

1. Enhance Simulation of Two-Way Arching Mechanisms:
   Although the current model incorporates 3D wall behavior, future developments should focus on improving the representation of two-way arching action, especially for walls with significant out-of-plane slenderness in both directions or those interacting with adjacent orthogonal components.
2. Develop a Nonlinear Analysis Framework:
   To better capture the progression of cracking and post-peak response, it is necessary to extend the current framework to include nonlinear material models and displacement-based analysis methods.
3. Integrate MATLAB Code into a Unified Platform:

The current MATLAB scripts are modular but disconnected. Consolidating them into a fully integrated, user-friendly platform will improve computational efficiency and usability for engineering applications.

4. Establish a Real-Scenario Database to Support Reduction Factor Calibration:

   A comprehensive database of experimental and field performance data should be compiled to calibrate empirical reduction factors. This would allow for more accurate alignment between theoretical design and actual behavior, especially for FRP systems.

REFERENCES

[1] P. R. Hornsby, "Historical development of composites," in *Composites in Engineering*, 2nd ed., Cambridge: Woodhead Publishing, 2000, pp. 1–14.

[2] M. Ashby and D. Cebon, *Materials: Engineering, Science, Processing and Design*, 3rd ed., Amsterdam: Elsevier, 2018.

[3] J. E. Gordon, *The New Science of Strong Materials*, Princeton: Princeton University Press, 2006.

[4] L. Nicolais and G. Carotenuto, *Composite Materials: A Vision for the Future*, Weinheim: Wiley-VCH, 2011.

[5] M. K. A. Ahmed et al., "Recent advances in composite materials for aerospace applications," *Composites Part B: Engineering*, vol. 202, pp. 108–120, 2020.

[6] R. M. Jones, *Mechanics of Composite Materials*, 2nd ed., Philadelphia: Taylor & Francis, 1999.

[7] S. Maiti, M. R. Islam, M. A. Uddin, S. Afroj, S. J. Eichhorn, and N. Karim, “Sustainable fiber-reinforced composites: A review,” Adv. Mater., vol. 35, no. 4, p. 2207767, 2023.

[8] Organization of American States, Building Guidelines Drawings: Section B – Concrete Construction, Department of Sustainable Development, OAS, 2004. [Online]. Available: https://www.oas.org/pgdm/document/building_guidelines/sectionb.pdf

[9] Degenkolb Engineers, Unreinforced Masonry Buildings, [Online]. Available: https://degenkolb.com/seismic-ordinances/unreinforced-masonry-buildings/. [Accessed: Jul. 1, 2025].

[10] NCREE, Overview of Retaining Wall Failures During the 1999 Chi-Chi Earthquake, Fig. 14, Natl. Center for Research on Earthquake Engineering, Taiwan, 2000.

[11] D. E. Alexander, “The L’Aquila earthquake of 6 April 2009 and Italian government policy on disaster response,” J. Nat. Resour. Policy Res., vol. 2, no. 4, pp. 325–342, 2010.

[12] L. Ascione, G. Mancusi, and F. Russo, “A unified approach for the design of FRP strengthening systems,” Composites Part B: Engineering, vol. 67, pp. 468–477, 2014.

[13] G. De Felice, “FRP systems for seismic strengthening of masonry structures: a review,” Journal of Composites for Construction, vol. 15, no. 5, pp. 731–743, 2011.

[14] A. Borri, A. Castori, M. Corradi, and A. Vignoli, “Retrofit of masonry panels with FRCM systems,” Composites Part B: Engineering, vol. 115, pp. 180–192, 2017.

[15] P. Ricci, F. Balsamo, and G. Verderame, “Experimental results on out-of-plane behavior of masonry walls strengthened with FRCM,” Materials and Structures, vol. 50, no. 1, pp. 1–14, 2017.
[16] T. C. Triantafillou and L. Koutas, “Innovative strengthening of URM walls using textile-based composites,” Engineering Structures, vol. 124, pp. 521–533, 2016.
[17] Ascione, L., De Felice, G., & De Santis, S. (2016). A qualification method for externally bonded Fibre Reinforced Cementitious Matrix (FRCM) strengthening systems. Composite Structures, 142, 110–119.
[18] Grande, E., Imbimbo, M., & Sacco, E. (2018). Modeling and analysis of FRCM strengthening systems for masonry structures. Composites Part B: Engineering, 141, 254–262.
[19] D'Ambrisi, A., Feo, L., & Focacci, F. (2013). Experimental analysis on bond between PBO-FRCM strengthening materials and masonry substrates. Composites Part B: Engineering, 44(1), 524–532.
[20] H. Toutanji, L. Zhao, and E. Anselm, “Verifications of design equations of beams externally strengthened with FRP composites,” J. Compos. Constr., vol. 10, no. 3, pp. 254–264, Jun. 2006, doi: 10.1061/(ASCE)1090-0268(2006)10:3(254).
[21] Ombres, L. (2014). Analysis of the bond between fabric reinforced cementitious mortar (FRCM) strengthening systems and masonry. Composites Part B: Engineering, 69, 418–426.
[22] Babaeidarabad, S., Arboleda, D., Loreto, G., & Nanni, A. (2014). FRCM strengthening of concrete masonry walls subjected to out-of-plane load. Construction and Building Materials, 72, 213–221.
[23] Raoof, S. M., Koutas, L. N., & Bournas, D. A. (2017). Textile-reinforced mortar (TRM) versus fiber-reinforced polymers (FRP) in flexural strengthening of RC beams. Construction and Building Materials, 151, 279–291.
[24] Triantafillou, T. C. (2016). Strengthening of existing masonry structures: Concepts and structural behavior. ACI Special Publication, SP-304.
[25] L. Koutas, Z. Tetta, D. A. Bournas, and T. Triantafillou, “Strengthening of concrete structures with textile reinforced mortars: State-of-the-art review,” J. Compos. Constr., vol. 22, no. 1, p. 04017107, Jul. 2018.
[26] De Felice, G., Aiello, M. A., Caggegi, C., Ceroni, F., De Santis, S., & Garbin, E. (2018). Structural applications of FRCM in strengthening masonry structures: a state-of-the-art review. Construction and Building Materials, 193, 233–248.
[27] Prota, A., Marcari, G., & Fabbrocino, G. (2017). Masonry strengthening with Textile Reinforced Mortars. Materials and Structures, 50, 1–14.

[28] Koutas, L., & Triantafillou, T. C. (2015). Use of textile reinforced mortar (TRM) as a new strengthening solution. Journal of Composites for Construction, 19(6), 04014076.
[29] Gattesco, N., & Boem, I. (2017). Experimental study on masonry vaults reinforced with Textile-Reinforced Mortar (TRM). Engineering Structures, 136, 138–148.
[30] Ascione, F., Berardi, V. P., & Giordano, A. (2018). Retrofit of masonry structures by innovative FRCM solutions. International Journal of Masonry Research and Innovation, 3(3), 183–206.
[31] Carloni, C., & Subramaniam, K. V. (2018). FRP versus FRCM composites for masonry strengthening: Review of recent research. ACI Special Publication, SP-330.
[32] Triantafillou, T.C., & Koutas, L. (2011). Textile-Reinforced Mortar (TRM) versus FRP as Strengthening Material of URM Walls: Out-of-Plane Cyclic Loading. Materials and Structures, 44(3), 593–606.
[33] Borri, A., Corradi, M., & Speranzini, E. (2011). In-plane shear strengthening of masonry panels with TRM. Construction and Building Materials, 25(12), 4375–4385.
[34] Ricci, P., Verderame, G.M., & Manfredi, G. (2013). Analytical modelling of out-of-plane behaviour of URM walls strengthened with FRP or FRCM systems. Engineering Structures, 56, 1127–1142.
[35] NR-DT 200 R2/2025 – Guide for the Design and Construction of Externally Bonded FRP Systems for Strengthening of Structures.
[36] CNR-DT 215/2018 – Instructions for the Design, Execution and Control of Strengthening Interventions of Structures Using FRCM Systems.
[37] Dawe, J.L. and Seah, C.K. (1989). "Out-of-plane resistance of concrete masonry infilled panels." Canadian Journal of Civil Engineering, 16(6), pp. 854–864.
[38] Kafle, B., Magenes, G., 41, M.C. (2015). "Evaluation of unreinforced masonry walls under blast loading using simplified analytical methods." Engineering Structures, 105, pp. 210–224.
[39] Griffith, M.C., Vaculik, J. (2007). "Cyclic testing of unreinforced masonry walls in two-way bending." Earthquake Engineering & Structural Dynamics, 36(6), 801–821.
[40] Doherty, K., Griffith, M.C., Lam, N.T.K., Wilson, J.L. (2002). "Displacement-based analysis for out-of-plane bending of seismically loaded unreinforced masonry walls." Earthquake Engineering & Structural Dynamics, 31(4), 833–850.
[41] Kafle, B., Magenes, G., Griffith, M.C. (2015). "Evaluation of unreinforced masonry walls under blast loading using simplified analytical methods." Engineering Structures, 105, 210–224.
[42] Chock, G., et al. (2013). “Tsunami-Resilient Building Design Considerations.” ASCE/SEI Structures Congress Proceedings, Pittsburgh, PA.

[43] N. Galati, E. Garbin, G. Tumialan, and A. Nanni, Design Guidelines for Masonry Structures: Out-of-Plane Loads (SP-230—16), Farmington Hills, MI: American Concrete Institute (ACI), 2016.

[44] N. Gattesco, I. Boem, and S. Conz, "Tensile Behavior of Steel FRCM Composites: Experimental Analysis and Analytical Modeling," *Fibers*, vol. 9, no. 8, p. 45, 2021.

[45] N. Gattesco, I. Boem, and S. Conz, "Experimental Investigation on the Bond Behavior of Steel FRCM Composites," Fibers, vol. 10, no. 8, p. 67, 2022.

[46] G. M. Verderame, A. Balsamo, P. Ricci, M. Di Domenico, and G. Maddaloni, "Experimental assessment of the out-of-plane response of strengthened one-way spanning masonry infill walls," Engineering Structures, vol. 256, p. 113943, 2022.

[47] S. M. Mosallam, "Out-of-plane flexural behavior of unreinforced masonry walls strengthened with FRP composites," *Composites Part B: Engineering*, vol. 38, no. 5–6, pp. 559–574, 2007.

[48] M. Griffith, D. Drysdale, and D. Lam, "Out-of-plane strengthening of unreinforced masonry walls with fibre-reinforced polymer sheets," *Australian Journal of Structural Engineering*, vol. 8, no. 3, pp. 207–219, 2007.

[49] G. P. F. Valluzzi, C. G. Papanicolaou, M. Triantafillou, "Out-of-plane strengthening of masonry walls with FRP composites," *Compos. Struct.*, vol. 59, no. 1, pp. 107–118, 2003.

[50] G. Tumialan, A. Nanni, D. Tinazzi, "Field evaluation of URM walls strengthened with FRP composites subjected to out-of-plane loading," *Symp. Concr. Concern Struct.*, vol. 327, pp. 22.1–22.14, 2001.

[51] G. M. Verderame, A. Balsamo, P. Ricci, G. Maddaloni, "Experimental assessment of the out-of-plane response of strengthened masonry infills," *Compos. Struct.*, vol. 225, pp. 111150, Sept. 2019.

[52] T. D'Antino, S. Manfredi, A. Cavaleri, G. Cosenza, "Experimental investigation of tensile and bond properties of carbon-FRCM composites for masonry strengthening," *Constr. Build. Mater.*, vol. 212, pp. 68–81, Nov. 2019.

[53] C. G. Papanicolaou, E. Seenan, M. Triantafillou, "Seismic retrofitting of unreinforced masonry structures with TRM jacketing," in *Proc. 1st Int. RILEM Conf. Textile Reinforced Concrete*, Iceland, 2006, pp. 341–350.

[54] P. Ricci, G. M. Verderame, A. Balsamo, "Experimental and numerical investigation of FRCM-strengthened masonry walls under out-of-plane loading," *Compos. Struct.*, vol. 258, p. 113278, June 2021.

alls strengthened with CFRP strips," Construction and Building Materials, vol. 278, p. 122367, 2021.
[55] D'Antino, T., Carozzi, F. G., Colombi, P., & Poggi, C. (2018). Out-of-plane maximum resisting bending moment of masonry walls strengthened with FRCM composites. Composite Structures, 202, 881–896.
[56] De Santis, S., De Canio, G., de Felice, G., Meriggi, P., & Roselli, I. (2019). Out-of-plane seismic retrofitting of masonry walls with Textile Reinforced Mortar (TRM) composites. Bulletin of Earthquake Engineering, 17(11), 6265–6300.
[57] Pradhan, B., Sarhosis, V., Ferrotto, M. F., Penava, D., & Cavaleri, L. (2021). Prediction equations for the out-of-plane capacity of unreinforced masonry infill walls based on a macro-element model parametric analysis. Journal of Engineering Mechanics, 147(11), 04021096.
[58] ICE Publishing. (2020). Masonry arch bridge assessment and arching action mechanics. Proceedings of the Institution of Civil Engineers – Bridge Engineering. ICE Virtual Library.
[59] Angel, R., Abrams, D. P., Shapiro, D., Uzarski, J., & Webster, M. (1994). Behavior of reinforced concrete frames with masonry infills. University of Illinois Engineering Experiment Station, Report No. UILU-ENG-94-2005.